TAMPEREEN TEKNILLINEN YLIOPISTO
TAMPERE UNIVERSITY OF TECHNOLOGY
Julkaisu 699 • Publication 699

Anu Juslin

Alignment of Cardiac Structures in [^{15}O]H_2O Perfusion PET Studies

Tampere 2007

Tampereen teknillinen yliopisto. Julkaisu 699
Tampere University of Technology. Publication 699

Anu Juslin

Alignment of Cardiac Structures in [^{15}O]H_2O Perfusion PET Studies

Thesis for the degree of Doctor of Technology to be presented with due permission for public examination and criticism in Tietotalo Building, Auditorium TB109, at Tampere University of Technology, on the 14th of December 2007, at 12 noon.

Tampereen teknillinen yliopisto - Tampere University of Technology
Tampere 2007

ISBN 978-952-15-1882-9 (printed)
ISBN 978-952-15-1976-5 (PDF)
ISSN 1459-2045

Abstract

Positron emission tomography (PET) with $[^{15}O]H_2O$ provides a method to measure quantitatively the myocardial perfusion *in vivo*. The quantification enables an objective and accurate way to compare studies acquired on different time occasions or under different conditions. The challenge in $[^{15}O]H_2O$ cardiac perfusion PET studies is the low contrast between cardiac structures in the images, because the tracer is freely diffusible. Furthermore, the contraction motion of the heart and the movement of the heart in the thorax, due to respiration, make the quantitative analysis even more difficult. In addition, the patient may move during the acquisition or the position of the patient may change between the studies. For these reasons, the goal of the thesis has been to develop and evaluate image analysis methods to improve the usability of $[^{15}O]H_2O$ myocardial perfusion PET studies for drug development and clinical diagnostics. In this thesis, a novel systemic process to align the studies to the same position is presented. Thanks to the alignment, the same regions of interest (ROIs) can be used in the analyses of the studies, ensuring that the comparison is carried out in equivalent myocardial segments. This increases the repeatability and accuracy of the quantification.

Because the heart position is not fixed in the thorax, the alignment should be carried out using cardiac structures instead of external landmarks or other thoracic structures. In this thesis, the independent component analysis (ICA) method was evaluated for the separation of the cardiac structures. For the alignment of the studies, an approach based on mutual information (MI) was developed. The difficulty in developing and improving the analysis of medical images is that reference values, i.e. golden standards, are not available, on which to base the comparison. In this thesis, one of the aims was to construct realistic simulated data, to be able to evaluate the developed approach. In the constructed simulated data, knowledge of the heart physiology, anatomy and function was combined in the measurement of the myocardial perfusion with PET and O-15-labeled water.

With the simulated data, it was possible to quantitatively evaluate ICA for the separation of the cardiac structures, as well the developed approach to align the studies. The cardiac structures were successfully separated with ICA under different perfusion levels, and with cardiac and respiratory motion, even with real human data. The results proved that the cardiac structures from different studies can reliably be extracted for the alignment. The quantitative evaluation of the developed approach proved that by

aligning the studies, the same ROIs can be used for comparative analysis of the studies. Furthermore, the alignment of the two studies could be carried out without the use of information from the myocardium, and thus the method is not affected by possible abnormalities in the myocardial tissue. The developed approach can be used, in practice, with real human studies to facilitate analysis of $[^{15}O]H_2O$ myocardial perfusion PET studies.

Acknowledgments

The research reported in this thesis was carried out at the Institute of Signal Processing, Tampere University of Technology during the years 2003-2007.

I am highly grateful to my supervisor Professor Ulla Ruotsalainen for guiding me trough the doctoral studies. Her continuous encouragement and support have inspired me along the way.

I would like to thank PhD Jussi Tohka for his guidance and support. I am also thankful to MSc Margarita Magadan-Mendez, for inspiring co-operation during these years. I owe my warmest thanks to PhD Jyrki Lötjönen for his contribution to this work. I want to express my sincere thanks to the co-authors and personnel from Turku PET centre, especially Professor Juhani Knuuti, Docent, PhD Kari Kalliokoski, MD, PhD Sergey Nesterov, and MSc Vesa Oikonen for the excellent collaboration. I also want to thank MSc Anthonin Reilhac (CERMEP, France) for his great help with simulations.

The reviewers of this thesis, Professor Pirjo Nuutila and PhD Koen Van Leemput deserve sincere thanks for their careful reading and constructive feedback of the manuscript of this thesis.

I want to express my gratitude to my colleagues in our research group, M^2oBSI, for their support and help. I would also like to thank my colleagues at the Institute of Signal Processing for creating an inspiring working environment.

The financial support provided by the Graduate School of Tampere University of Technology, Tampere Graduate School of Information Sciences and Engineering (TISE), TEKES Drug 2000 technology program, the Academy of Finland (project no. 213462, Finnish Centre of Excellence program (2006-2011)), the Ulla Tuominen's foundation, the Finnish Konkordia foundation, the Finnish Foundation for Economics and Technology (KAUTE), and the Finnish Cultural Foundation of Pirkanmaa are gratefully acknowledged.

I thank my friends for supporting me during the studies. I wish to thank my parents and sisters for their encouragement and love during my life and studies. Finally, I express my warmest thanks to my husband Osku and our daughter Lumi.

Tampere, November 2007

Anu Juslin

Supervisor	Professor Ulla Ruotsalainen Institute of Signal Processing Tampere University of Technology
Instructor	Jussi Tohka, PhD Institute of Signal Processing Tampere University of Technology
Pre-examiners	Professor Pirjo Nuutila Turku PET Centre and Department of Medicine University of Turku
	Koen van Leemput, PhD Martinos Center for Biomedical Imaging Massachusetts General Hospital and Harvard Medical School and MIT Computer Science and Artificial Intelligence Laboratory
Opponent	Isabelle Magning, PhD CREATIS-LRMN Insa School, University Claude Bernard of Lyon

Tampere University of Technology
Department of Information Technology
Institute of Signal Processing
Turku PET centre

Contents

Abstract iii

Contents vii

List of publications ix

Symbols and Abbreviations xi

1 Introduction 1

2 Myocardial Perfusion Imaging 3
- 2.1 Myocardial Perfusion . . . 3
- 2.2 Methods to Image Myocardial Perfusion . . . 5
  - 2.2.1 Myocardial Perfusion Imaging with PET . . . 6
  - 2.2.2 Quantification of Myocardial Perfusion . . . 7

3 Movement of Heart During Imaging 11
- 3.1 Heart Motion During Contraction . . . 12
- 3.2 Respiratory Movement of Heart . . . 14
- 3.3 Patient Movement During Imaging . . . 15
- 3.4 Transmission - Emission Misalignment . . . 15

4 Simulation of Cardiac PET Data 17
- 4.1 Simulation of Anatomy and Movement of Heart . . . 17
- 4.2 Simulation of Perfusion . . . 18
- 4.3 Simulation of PET Acquisition . . . 19

5 Alignment of Cardiac Structures 21
- 5.1 Alignment of Cardiac Images . . . 22
- 5.2 Developed and Evaluated Methods . . . 23
  - 5.2.1 Segmentation of Cardiac Structures . . . 24
  - 5.2.2 Alignment of Cardiac Structures with MI . . . 26

6 Experiments and Results **29**
6.1 Simulated Data in this Work 29
6.2 Human Data in this Work 30
6.3 Evaluation of Results 31
6.4 Results 32

7 Discussion **37**
7.1 Author's Contribution 40
7.2 Concluding Remarks 40

8 Summary of Publications **43**

References **45**

Publications **57**

List of publications

This theses is composed of the introductory part and the following original publications. These are referred to in the text as [Publication $*$], where $*$ denotes the corresponding number of the publication.

I A. Juslin, A. Reilhac, M. Magadan-Mendez, E. Alban, J. Tohka and U. Ruotsalainen, "Assessment of separation of functional components with ICA from dynamic cardiac perfusion PET phantom images for volumes extraction with deformable model," in *Third International Conference on Functional Imaging and Modeling of the Heart (FIMH'05)*, Lecture Notes of Computer Science, vol 3504, 2005, pp. 338–347.

II A. Juslin, and J. Tohka, "Unsupervised segmentation of cardiac PET transmission images for automatic heart volume extraction," in *Proceedings of the 28th Annual International Conference of the IEEE Engineering in Medicine and Biology Society (EMBC'06)*, New York, USA, August 30 – September 3, 2006, pp. 1077–1080.

III M. Magadan-Mendez, A. Juslin, SV. Nesterov, J. Knuuti, and U. Ruotsalainen, "ICA based automatic segmentation of dynamic $H_2^{15}O$ cardiac PET images," in *IEEE Transaction on Information Technology in Biomedicine*, accepted, 2007.

IV A. Juslin, J. Lötjönen, SV. Nesterov, J. Knuuti, and U. Ruotsalainen,"Alignment of 3-dimensional cardiac structures in O-15 labeled water PET emission images with mutual information," *Journal of Nuclear Cardiology*, vol 14, no.1, 2007, pp. 82–91.

V A. Juslin, J. Tohka, J. Lötjönen, and U. Ruotsalainen, "Comparison of image segmentation and registration based methods for analysis of misaligned dynamic $H_2^{15}O$ cardiac PET images ," in *Proceedings of the IEEE Medical Imaging Conference (MIC2006)*, San Diego, USA, December 1–4, 2006, pp. 3200–3204.

[Publication I] and [Publication III] will also be part of the Ph.D. thesis of M. Magadan-Mendez. The original publications that have been published are reproduced with the permission of the copyright holders.

Symbols and Abbreviations

$2D$	two-dimensional
$3D$	three-dimensional
$[^{15}O]H_2O$	water labeled with positron emitting oxygen (^{15}O)
α	tissue fraction; grams of perfusable tissue per milliliter of ROI [ml/ml]
β	recovery coefficient of left-ventricular ROI [ml/ml]
C_a	concentration of the tracer in arterial plasma [kBq/ml]
C_v	concentration of the tracer in venous plasma [kBq/ml]
C_t	concentration of the tracer in tissue [kBq/ml]
CAD	coronary artery disease
CE	contrast echocardiography
CFR	coronary flow reserve
CT	computed tomography
DM-DSM	deformable models with dual surface minimization
ECG	electrocardiogram
f	organ blood flow [ml/min/g]
FBP	filtered back projection
FDG	Fluoro-2-deoxy-D-glucose, a glucose analog labeled with positron emitting ^{18}F
FOV	field of view
ICA	independent component analysis
K_1	transport of a tracer into a cell
k_2	transport of a tracer from a cell
LV	left ventricle
MBF	myocardial blood flow
MCAT	mathematical cardiac torso phantom
MI	mutual information
MRI	magnetic resonance imaging
NCAT	non-uniform rational b-lines (NURBS)-based cardiac torso phantom
NMI	normalized mutual information

OSEM	ordered-subsets expectation maximization
p	partition coefficient of water [ml/ml]
PET	positron emission tomography
PVE	partial volume effect
ROI	region of interest
RV	right ventricle
SPECT	single photon emission tomography
t	time
TAC	time activity curve
V_a	arterial blood volume; volume of arterial vascular space (including the spill-over from the chamber) in ROI [ml/ml]
VOI	volume of interest

Chapter 1

Introduction

In the western world, ischemic heart disease is the leading cause of death [73]. Decreased perfusion in the myocardium is the first sign of the disease [16]. The disease can be treated either by use of drugs or by-pass surgery. To develop new drugs for ischemic heart disease or assess the effectiveness of therapeutic interventions, a quantification of the myocardial perfusion is needed. The quantification provides an objective way to compare the results, and enables the comparison of large amounts of data from different subjects, acquired in different centers (multi-center study). In clinical diagnostics, noninvasive quantification of myocardial blood flow (MBF) can be used to assess the need of medical therapy or surgery [11].

Positron emission tomography (PET) with O-15-labeled water is an attractive method to measure the myocardial perfusion, because $[^{15}O]H_2O$ is almost freely diffusible, has a short half-life, its kinetics is related to the blood flow, and biological behavior can be modeled with a simple one-tissue compartment model. Quantification of the perfusion requires dynamic imaging, where the distribution of the radiotracer is followed over time at short time intervals, called time frames. The short half-life of O-15-labeled water enables repeated measurements under different conditions, like rest and stress, in a short time window. This is important for the intervention studies, e.g. drug studies, where the effects of medication and training on metabolism, function and efficiency of the whole myocardium are studied. In addition, the impaired blood flow at rest compared to the stress indicates possible stenosis in the coronary arteries. The ratio between the rest and stress perfusion is also used to measure the coronary flow reserve (CFR), the ability of the vascular bed to alter its resistance. In this thesis, the emphasis is on the cardiac perfusion PET studies with O-15-labeled water.

To compare the perfusion values from different studies, it needs to be ensured that the quantitative and visual analysis have been done in equivalent myocardial regions. In brain images, it can be assumed that the position and orientation of the brain is not changed inside the skull, but the heart does not have a fixed position in the thorax. The heart position changes due to the cardiac contraction, respiration, and patient movements. Also the repositioning of the patient to exactly the same position in different

studies is difficult. To ensure that the analysis is done in equivalent regions, the studies can be aligned to the same position before the comparisons.

The alignment, also called registration, is a common image processing task in medical imaging. Especially in brain imaging, a number of registration algorithms have been developed [39, 65]. Because of the nonrigid heart and respiration motions in the thorax region, the cardiac image registration is a more complex problem than brain image registration [67], . In addition, there are no anatomically accurate landmarks in the heart region, which could be used for the alignment. The alignment of cardiac PET images has been done using external skin markers [70], body and lung surfaces [66], and transmission images [6, 74]. However, these methods do not guarantee the alignment of the heart region, and therefore the best choice for the alignment is to use the cardiac structures [51, 98].

The goal of this thesis is to improve the analysis of the $[^{15}O]H_2O$ cardiac perfusion PET studies. To meet this, a novel process to align two $[^{15}O]H_2O$ perfusion PET studies using cardiac structures is developed. The alignment of repeated studies provides the possibility to use the same regions of interest (ROIs), thus increasing the repeatability and accuracy of the quantification. The challenge in the O-15-labeled water images is the poor contrast between the blood and tissue, because the O-15-labeled water circulates in the blood as well as diffuses into the tissues [8]. Due to this, the dynamic O-15-labeled water images have to be segmented first, so that the cardiac structures can be applied for the alignment. In this thesis, an independent component analysis (ICA) based method to separate the cardiac structures from dynamic $[^{15}O]H_2O$ cardiac images is evaluated.

The problem of evaluating the developed methods with real data is that the correct result (ground truth) is not known, and there are no generic image processing methods for use with different kinds of cardiac data. Nevertheless, the performance of image processing methods can be quantified by use of realistic simulations for a image acquisition and phantom images to describe the human anatomy. In the simulated data the ground truth values of the anatomy and physiological functions are known. The real challenge in the simulation of cardiac emission images is to realistically simulate the anatomy, physiology, and also the movement of the cardiac structures. In this thesis, one of the aims is to construct realistic simulated data based on the knowledge of the physiology, anatomy, and function of the heart as well on the measurement of the myocardial perfusion with PET. The construction of the simulated data will also provide a ground to improve the analysis of the $[^{15}O]H_2O$ cardiac perfusion PET studies with image analysis methods.

Chapter 2

Myocardial Perfusion Imaging

In physiology, perfusion is the process delivering nutritive blood to a capillary bed in a biological tissue. Each tissue controls its own local blood flow in proportion to its metabolic needs [33]. The heart responds to the need for blood flow in different organs by controlling the cardiac output. When the need for cardiac output increases during stress, also the need for blood flow to the heart muscle, the myocardium, increases. A decreased perfusion in the myocardium during stress is the first sign of an ischemic heart disease, followed by wall motion abnormalities. Decreased cardiac output can lead to cardiac failure and even to death, because the heart is incapable of contracting sufficiently to force enough blood into the arterial tree.

Noninvasively the perfusion can be measured with different imaging modalities. In this chapter, the physiological background of the myocardial perfusion is briefly introduced and different imaging techniques to measure the myocardial perfusion are reviewed. The left side of the heart is the most studied part of the heart and all the values are given for it, if not otherwise mentioned (Fig. 2.1). Because the aim of the thesis is to improve the repeatability and accuracy of the quantitative analysis of the myocardial perfusion studies, the emphasis is on the perfusion measurement with PET and $[^{15}O]H_2O$.

2.1 Myocardial Perfusion

The heart has two main coronary arteries, left and right, through which the heart receives its nutritive blood flow (Fig. 2.1). Commonly in the literature, the terms blood flow and perfusion are used in parallel, although the blood flow strictly means the flow of the blood in the vessels. The myocardial perfusion depends on the perfusion pressure and the resistance in the vascular bed. The blood flow in the coronary arteries is controlled by several mechanisms; autoregulation, extravascular compressive forces, and metabolic, neural, endothelial, and myogenic control [12]. The primary control is the local metabolism, the response of cardiac muscle to its need for nutrition, especially for oxygen. Although the mass of the heart is only 0.5 % of the total body weight, the

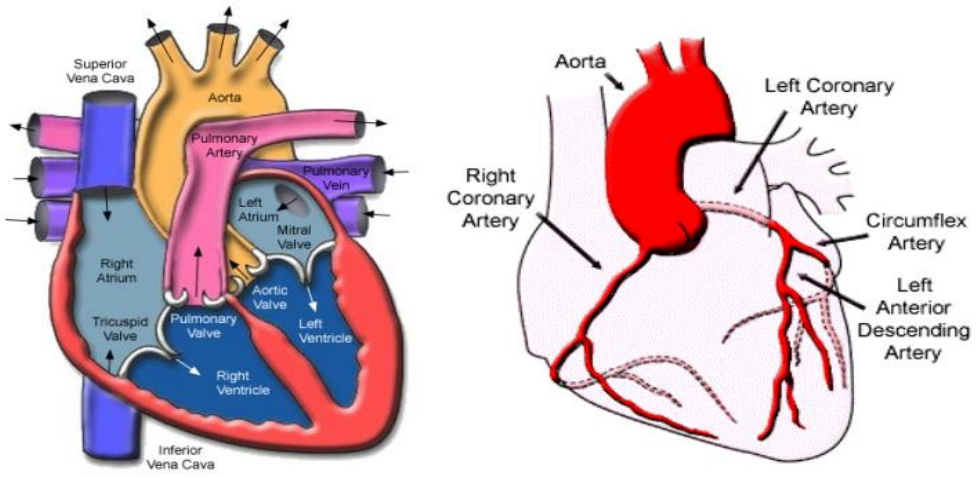

Figure 2.1: The anatomy of the heart (left) and the location of coronary arteries (right). ©Texas Heart Institute, reprinted with permission from (www.texasheart.org).

heart consumes 10 % of the whole body oxygen consumption in the resting condition.

The normal myocardial perfusion is on average 0.7 ml/min/g [33] at rest (basal), but may vary even from 0.6 to 2.4 ml/min/g [19]. During exercise or pharmacological stress (hyperemic), the perfusion increases three to fivefold in healthy subjects. However, the perfusion varies between subjects, and it is heterogenous over the cardiac muscle, making it difficult to define global normal limits. To assess the possibility of having coronary artery disease (CAD) the impaired blood flow between rest and stress states has been documented to predict possible stenosis in the coronary arteries. The perfusion can be normal at rest eventough the size of the stenosis is 90 % of the normal arterial diameter [22]. Measuring the perfusion at rest and after pharmacological stress also allows measurement of the CFR, which is the ratio between hyperemic and resting flows. CFR reflects the ability of the vascular bed to alter its resistance.

CAD occurs when the arteries that supply blood to the heart muscle (the coronary arteries) become hardened and narrowed, by plaques [33], which block, or partially block, the blood flow to the muscle. The most common reason for this is atherosclerosis. The reduction of blood flow to the muscle decreases the perfusion in the muscle, especially after stress as mentioned above. The reduced perfusion is followed by ischemia, which induces regional functional abnormalities, and finally may cause the patient some chest pain (angina). In addition, a heart attack is a result of reduced blood flow and oxygen to the muscle. Usually, the subendocardial muscle gets damaged first, because of the greater compression force of the myocardial muscle in the inner layers, which compress the subendocardial vessels more than the outer ones [33].

2.2 Methods to Image Myocardial Perfusion

Coronary angiography is considered as the golden standard method to diagnose the CAD [16]. The method is based on X-ray imaging and special dye (contrast agent) to visualize the blood flow in the vessels. The disadvantage of the method is that a catheter needs to be inserted into a vessel in the groin or arm, making the method very invasive. In addition, although the stenoses are identified from the images, the perfusion in the myocardium can not always be defined. Myocardial perfusion can be less invasively measured by the use of nuclear cardiology, contrast echocardiography (CE), magnetic resonance imaging (MRI), and computed tomography (CT).

Nuclear cardiology, by the use of single photon emission tomography (SPECT) or PET, is the most widely used noninvasive method to image the myocardial perfusion [23]. In nuclear cardiology small amounts of radioactive material, physiologically interesting compounds and radiopharmaceuticals, are used to obtain physiological information about the heart. Today, cardiac MRI and CE are also used increasingly in diagnosis. The advantage of these methods over nuclear cardiology is that no radiation is needed. The strength of CE is the wide availability and ease of use, but the weakness is that the method is heavily operator-dependent and the quality of images is poor. The high spatial resolution and contrast are the advantage of cardiac MRI; making it possible to differentiate the sub-endocardial and sub-epicardial regions. MRI and CE will be used more widely as a clinical tool for the assessment of myocardial perfusion, but the contrast media, hardware, software, and quantitative analysis still need improvements and wider clinical tests [23].

Due to the lower costs and availability, SPECT has been used more than PET. SPECT is a technique which measures the emission of single photons of a given energy from radioactive tracers. Perfusion imaging with SPECT can be done with tracers like Thallium-201 (Tl-201), and Technetium-99m sestamibi (Tc-99m). Both tracers have a relatively long physical half-life (Tl-201:73 hours , Tc-99m:6 hours) and the perfusion image is based on the high first-pass extraction of the tracer in the myocardium. The disadvantages of using SPECT has traditionally been the qualitative nature of the method and the problems of correcting the photon attenuation in the thorax [84]. Currently, the SPECT imaging is done with ECG-gating, providing the possibility to assess the left ventricular ejection fraction and wall motion abnormalities at the same time as the perfusion [52].

The SPECT, MRI and CE techniques are good and cost-effective methods for diagnostic purposes. However, PET enables measurement of quantitative values of myocardial blood flow in the units of ml/min/g of tissue, providing a powerful tool for drug and treatment development. PET has also been used as reference method to evaluate the performance of the other methods [26, 85]. The quantification of the perfusion gives us an objective way to compare the results. The decreased perfusion in the myocardium at stress compared to the rest state can be diagnosed by visual assessment, which is a commonly used method to analyze the SPECT images. However, to define

whether the new drug has an effect on the perfusion, visual assessment is not accurate and objective. In addition, to define the proper dose, it is important to quantitatively calculate the responses. The quantification enables the comparison of large amounts of data from different subjects, acquired even in different centers (multi-center study), and to make comprehensive conclusions on the efficacy of the intervention. In diagnosis, the quantification of the perfusion provides sensitive criteria for the physiological significance of CAD. Noninvasive quantification of MBF can be used to determine the need of medical therapy or catheterization [11].

2.2.1 Myocardial Perfusion Imaging with PET

PET is a method which gives the possibility to measure regional physiological function by tracing the biological compounds, which have been tagged with positron emitting isotopes. Unlike SPECT, PET is based on the detection of pairs of photons created in an annihilation of a positron and an electron. The unique advantages of PET is the possibility to measure quantitatively concentrations of tracers in the tissue; this follows from the possibility to measure the attenuation of the photons accurately in the body, together with the nature of positron annihilation. The PET acquisition is composed of the measurement of an attenuation with transmission scan or CT and an emission scan. In myocardial perfusion imaging the most commonly used tracers are O-15-labeled water, N-13-labeled ammonia and the cationic potassium analog rubidium 82 (Rb-82). The physical half-life for these tracers are 2.1, 10 and 1.3 minutes respectively [10].

Both N-13-labeled ammonia and Rb-82 are partially extracted and they are retained in the myocardium for varying periods of time. The extraction of these tracers in the myocardium is nonlinear and inversely related to the blood flow. In contrast, O-15-labeled water is an almost freely diffusible tracer, its kinetics is related to the blood flow, and it is metabolically inert. O-15-labeled water can be said to be an almost ideal tracer for the assessment of myocardial blood flow (MBF) over a wide flow range [9]. The challenge of O-15-labeled water is that the tracer is distributed both to the vascular space and the myocardium, making the visualization of the myocardium difficult (Fig. 2.2). Due to the short half-life of $[^{15}O]H_2O$, repetitive measurements under different conditions can be performed within a reasonable time (10-15 minutes time intervals). Because the possible hypoperfusion may be seen only during stress, physical or pharmacological, the perfusion is measured first at rest (basal) and then at stress (hyperemic). In PET the stress test is primarily performed using pharmacological stress, dipyridamole or adenosine. One $[^{15}O]H_2O$ dynamic cardiac study usually lasts 6 minutes, with time-frames of 2-5 seconds in the beginning and longer 30 second time-frames at the end of the acquisition.

PET enables the study of both perfusion and metabolism of the myocardium. The metabolic imaging is usually performed using glucose analogue ^{18}F-2-deoxy-2-fluoro-D-glucose (FDG) tracer, which can be used to assess the viability of the myocardial tissue. By imaging both the perfusion and the glucose uptake of the heart, it is possi-

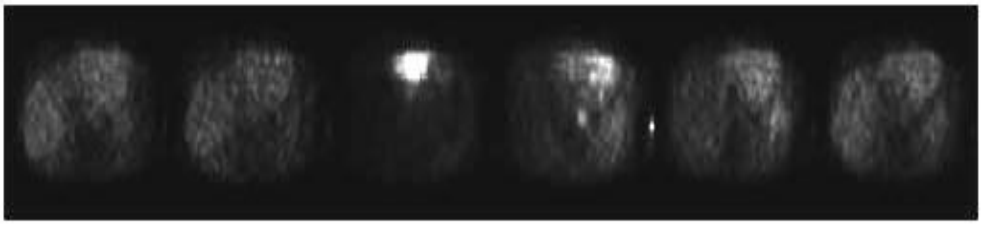

Figure 2.2: Example of transaxial slice of cardiac PET study at different time points from injection of $[^{15}O]H_2O$ (after 5 s, 25 s, 50 s, 80 s, 160 s and 280 s.)

ble to diagnose more accurately the patients' need for further treatment. From these two studies, it is possible to identify three different patterns: (1) both perfusion and metabolism are normal, (2) normal or augmented metabolism but reduced perfusion, or (3) both perfusion and metabolism are reduced [10]. Mismatch between perfusion and metabolism indicates viable but ischemic myocardium, which can still be returned by re-vascularization to normal contractility.

2.2.2 Quantification of Myocardial Perfusion with PET and $[^{15}O]H_2O$

Quantitative estimates of regional perfusion values with O-15-labeled water can be calculated using a mathematical model, which describes the biological behavior of the administrated radiopharmaceutical in the blood and myocardium over time. These models are based on compartment modeling, which describes the state of the tracer in a steady state biological system. The interest is, e.g. in a transfer of the tracer from one state to another. Because O-15-labeled water is almost freely diffusible and its kinetics is related to the blood flow, a simple one-tissue compartment model can be used (Fig. 2.3). The perfusion with O-15-labeled water is quantified using principles derived by Kety for the analysis of exchange of inert gas between the blood and tissue [8, 10]. The blood flow (f) is equal to the difference between the tracer entering and the tracer leaving the tissue:

$$\frac{dC_t(t)}{dt} = f(C_a(t) - C_v(t)), \tag{2.1}$$

where $C_t(t)$ is the tissue radioactivity concentration (kBq/ml); f is the blood flow per unit per tissue (ml/min/g); $C_a(t)$ is the arterial radioactivity concentration (kBq/ml); $C_v(t)$ is the venous radioactivity concentration (kBq/ml). Using the basic assumption that the $C_v(t)$ is the same as the $C_t(t)$ corrected with the partition coefficient p (ml/g), then the single compartment model for O-15 labeled water can be solved from the following differential equation:

$$\frac{dC_t(t)}{dt} = f(C_a(t) - \frac{1}{p}C_t(t)). \tag{2.2}$$

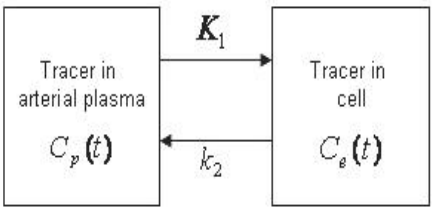

Figure 2.3: One-tissue compartment model. The parameters K_1 and k_2 correspond to the transport of the tracer in and out of the cell. The extraction of the water in the tissue is assumed to be 1, i.e. $K_1 = f$ and $k_2 = f/p$ [8, 10].

The partition coefficient is the ratio between the water content in the tissue and the water content in the whole blood. The tissue radioactivity concentration is then:

$$C_t(t) = fC_a(t) \otimes e^{-\frac{f}{p}t}, \tag{2.3}$$

where $\otimes$ denotes the convolution.

To calculate the flow, the time-activity curves (TACs) for the arterial blood pool and the myocardial tissue are measured from dynamic PET data. TAC describes the behavior of the tracer over time in the tissue. To ensure true quantification, accurate TACs need to be derived from the data. The TACs are derived from ROIs, which are drawn over the myocardium and left ventricle (LV). Unfortunately, the measured data are affected by the acquisition process (randoms, scatter, dead time, and normalization), image reconstruction and motion of the heart. In addition, due to the limited spatial resolution of the measurement compared to the small thickness of the structures of interest, so called partial volume effect (PVE) is caused, which usually results in underestimations of the true value. On the contrary, the spill-over of the radioactivity from the high activity area to surrounding areas causes overestimation of the true value. The PVE changes the scale and the spill-over changes the shape of the TACs. Using appropriate model these changes can be corrected [42].

In this work, a model that is based on the one-tissue compartment model, including PVE, and spill-over corrections, was used to calculate MBF [42, 44, 45, 72]. The model takes into account the underestimation of the MBF values due to cardiac wall motion and PVE using the concept of tissue fraction (α). Tissue fraction is the ratio of the mass of perfusable tissue within a given ROI to the volume of that ROI. In addition, the spill-over from the ventricle to the myocardium and vise versa, are corrected. The measured radioactivity concentration in a selected myocardial ROI is:

$$ROI_{myo}(t) = \alpha f C_a(t) \otimes e^{-\frac{f}{p}t} + V_a C_a(t), \tag{2.4}$$

where V_a is the arterial blood volume in a ROI and the radioactivity concentration in a selected LV ROI is:

$$LV(t) = \beta C_a(t) + (1-\beta) f C_a(t) e^{-\frac{f}{p}t}, \tag{2.5}$$

where the β is the recovery coefficient of LV ROI. The β can be measured from a separate blood volume scan. Solving equations 2.4 and 2.5 gives

$$ROI_{myo}(t) = (\frac{\alpha}{\beta} - \frac{(1-\beta)}{\beta^2} V_a) f LV(t) \otimes e^{-(\frac{1}{\beta} - \frac{(1-\beta)}{\beta})ft} + \frac{V_a}{\beta} LV(t), \tag{2.6}$$

and

$$C_a(t) = \frac{1}{\beta} LV(t) - \frac{(1-\beta)}{\beta^2} f LV(t) \otimes e^{-(\frac{1}{\beta} - \frac{(1-\beta)}{\beta})ft}, \tag{2.7}$$

The model parameters f, α, and V_a can be estimated using nonlinear fitting. The model is first fitted to a large ROI, covering the whole myocardium around the LV. With the found parameters, the arterial blood curve $C_a(t)$ can be calculated, which is then used to estimate the regional perfusion values in different locations of the myocardium, e.g. in the septum [72]. To calculate the quantitative blood flow values, the fixed partition coefficient p can be a problem in diseased tissue, because of the spill-over from the right ventricle to the left side, especially in the septum [104]. The model also assumes homogenous flow over the ROI, which may not be true.

To calculate and compare the quantitative values from different studies, it needs to be ensured that the values have been calculated from equivalent regions. The optimal position of the ROIs decreases the effects of bias and variance to the model parameters [38]. If the blood pool fraction is different between the image sets due to the different position of the ROIs, the quantitative values are not comparable. Manually, it is difficult to draw ROIs in the same position between 3D image sets acquired at different times or under different conditions. The patient may not be in the same position so that the heart is located in different transaxial slices between the studies. When comparing image sets acquired at rest and stress, the images may look different, because of the different intensity scale, making the definition of the borders of the myocardium difficult.

Chapter 3

Movement of Heart During Imaging

The circulation maintains an appropriate environment in our body. The function of the circulation is i.e. to transport substances to and from tissues and to conduct hormones from one part of the body to another [33]. The heart is the force, a pump, which moves the blood through the circulation. It is composed of two separate pumps: a right heart that forces out the blood through the lungs (pulmonary circulation) and a left heart that forces out the blood through the peripheral organs (systemic circulation). The cardiac cycle consists of events that occur from the beginning of one heart beat to the beginning of the next. It has two main phases, relaxation and contraction. The relaxation phase is named the diastole and the contraction phase the systole. During the diastole, the heart fills with blood and during the systole the blood is forced out into the circulation. The heart contracts almost 3 billion times in a life time [33].

The heart is located within the mediastinum in the thorax and bordered laterally by the lungs. Due to this, the heart also moves because of respiration. Because the position of the heart is not fixed, like the position of the brain inside the skull, the orientation and location of the heart may change depending on the position and condition of the patient. In addition, the position of the heart in the cardiac images may change because of patient/subject movement during the acquisition. The movement of the heart during the cardiac emission imaging can be illustrated with a 3-layer coordinate system (Fig. 3.1). The three coordinates are $heart$, which defines the contraction motion of the heart, $body$, which defines the movement of the heart in the thorax because of respiration, and img, which defines the heart position in the image field of view (FOV), due to the position of the patient/subject.

The directions and magnitudes of the motion can be studied with anatomical imaging techniques like MRI with magnetic tagging [4, 112], CT, and echocardiography [28]. The spatial and time resolution of these imaging techniques are better than in nuclear cardiology methods; especially MRI provides good anatomical images even with $1\ mm$ resolution and excellent contrast between the blood and the myocardium. The

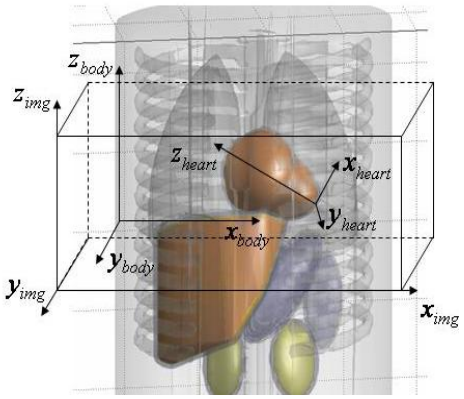

Figure 3.1: Coordinate system for the heart movement during cardiac emission imaging. The origin for the $heart$ coordination is the apex of the heart, the origin for the $body$ coordination can be defined in the surface of the thorax, and the origin of the img coordination is the corner of the first transaxial slice of the 3D image.

aim of this chapter is to provide an anatomical and functional background the the heart, and to discuss the limitations of the cardiac emission imaging caused by the movement of the heart.

3.1 Heart Motion During Contraction

The heart forces the blood out into the circulation by contracting. During the contraction the heart walls thicken, the heart shortens in the long-axis direction from base to apex, and the heart muscle twists around its long-axis (Fig. 3.2). The heart muscle, the myocardium, is about 12 mm thick on the left and 5 mm on the right side. The atria are only 2 mm thick. The whole left side of the myocardium can be considered to be almost uniform in thickness expecting for the apical region, which is only a few millimeters thick.

At rest, the volume of the normal ventricle is about 120 ml at end-diastole and decreases about 70 ml during systole [33] (Fig.3.3). At stress, the end-diastolic volume increases and the end-systolic volume decreases, producing an almost two times greater output volume. If the heart would be modeled as a sphere, the change of the volume would only cause a roughly 1 mm change in the radius at rest and less than a 2 mm change at stress. But the shape of the heart and its deformation during the cardiac cycle is much more complex. Using tagged MRI, an average 13 mm move of the valvular plane from base to apex has been measured. The movement decreases towards the apex, which can be considered to be almost static along the long-axis. During contraction, the heart wall thickens in normal subject 3-5 mm in the left ventricle wall [86], being greatest at the apex [89]. The twisting motion is counterclockwise in

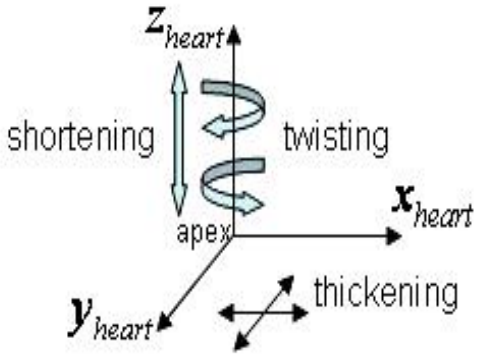

Figure 3.2: The heart motion due to the contraction. Because the apex of the heart is quite static point during the contraction of the heart muscle, it is defined to be the origin of the $heart$ coordination system.

the apex during the systole, and at the base, the direction is changed at the end of the systole. Meanwhile, the middle part of the ventricle is almost static [61]. In addition, the magnitude of the twisting changes along the left ventricular wall, from 20 degrees at the lateral wall, to 4 degrees at the septum. There are also differences in epicardium and endocardium torsion. Patients with cardiac disease have abnormalities in the regional contraction. It has been show that an abnormal heart twists more than a healthy heart to compensate for the inability to thicken as much as the healthy heart [75].

The contraction of the heart blurs the images and may cause bias in the regional estimates of blood flow [38, 93, 95]. In addition, the motion of the heart may lead to misquantification and causes some artificial defects on myocardial images. Because the motion is not similar in the whole left myocardium, the effects may vary spatially along the direction of the motion. In dynamic PET studies, the frame time is longer than one cardiac cycle, which in a normal person is $1s$ at rest and during stress the length of the cycle decreases even further. For this reason, only the average shape and location of the myocardial wall in dynamic emission tomography images can be seen. The problem with PET is also that the spatial resolution, which is optimally around 4 mm in cardiac PET images [35], would make a detection of the contraction motion difficult. It is also possible to detect the cardiac motion from PET images with cardiac gating, where the cardiac cycle is divided into shorter time frames based on the electrocardiogram (ECG) signal [51]. However, the gating is not feasible for O-15-water studies, because of the short half-life and rapid washout of the tracer from the myocardium.

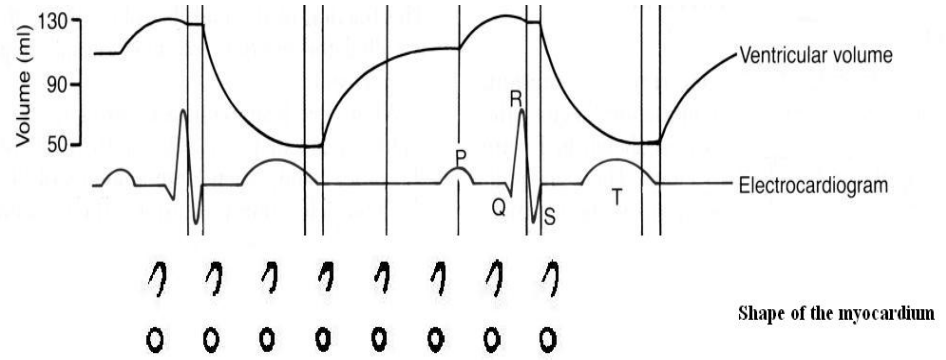

Figure 3.3: Events of the cardiac cycle for left ventricular function and anatomy, changes in the ECG, ventricular volume and shape of the ventricle.

3.2 Respiratory Movement of Heart

Because of the long acquisition times, it is not possible for a patient/subject to hold his/her breath during the emission tomography acquisition, unlike in X-ray imaging or cardiac magnetic resonance imaging. The normal breathing cycle, from full expiration throughout full inhalation back to full expiration normally lasts 3-5 seconds [71]. Due to the breathing, the heart is moving in a sinusoidal fashion, depending on the depth and frequency of the breathing. If the breathing frequency changes during the study also the movement of the heart changes. It has been measured that the heart apex moves on average 7-15 mm due to the breathing in the direction of the z_{body}-axis , 3-5 mm in the direction of the y_{body}-axis, and 2-3 mm in the direction of the x_{body}-axis [15, 58, 102]. The movement of the heart in the z_{body}-axis direction is linearly related to the diaphragm motion, but is smaller in magnitude. The respiration movement has greater effect on the apex region, which moves up and down on the top of diaphragm. However, it has been suggested that the heart movement, because of respiration, is more complex than just a 3D translation, based on the displacement of the coronary arteries [90]. In addition, the magnitude of the movement may change locally in the myocardium.

Another factor related to respiration is called 'cardiac creep', which has been explained to be caused by changes in respiration depth and changes in volume and distribution of the air in the lungs during the acquisition [29, 76, 83]. This phenomenon has been recognized, especially in the acquisitions after physical exercise, which is commonly used in stress SPECT studies. The magnitude of the creeping can be a few centimeters in the direction of the z_{body}-axis (Fig. 3.1).

Like heart motion, the respiration movement blurs the cardiac emission tomography images, and may lead to wrong quantification of the perfusion values. Similarly to using ECG gating, the respiration motion effects can be decreased with gating. The

respiratory gating can be done with the use of optical tracking, different kinds of belts, or oxygen masks [15, 58, 71]. The motion information can then be used to discard part of the data, to transform the sinogram or the list-mode data, or to perform the movement compensation during the iterative reconstruction [59].

3.3 Patient Movement During Imaging

Due to the long acquisition times in emission tomography, several minutes in a $[^{15}O]H_2O$ study, it is likely that the patient/subject cannot stay still the whole scanning time. This voluntary movement is difficult to predict and quantify, because the whole patient/subject may translate or rotate at various times during the scanning in the img coordinates (Fig. 3.1). The movement may occur during one time frame, or between the time frames. This movement directly affects to the heart orientation and also to the position in the image FOV. With the use of external markers in dynamic O-15-labeled water cardiac studies it was found that patient movement occurred in 18% of the time frames at rest, in 45% of the time frames during pharmacological stress, and in 80% of the time frames when physical exercise was performed during the acquisition [70]. The heart position may also change between the studies depending on the condition of the patient. Also the repositioning of the patient to exactly the same position on different occasions is difficult.

The patient movement can be detected using external markers [53, 70], or using the acquired data directly [24, 37, 91, 92, 98] In addition, attenuation scans have been proposed to be used to detect the misalignment of two scans [6, 74]. Especially in SPECT imaging, the patient/subject movement between camera rotations produces problems [20, 21, 27, 31, 32]. The patient movement can lead to misquantification and artificial defects. The visual and quantitative comparison of two image sets becomes difficult, and the same ROIs cannot be used in the analysis. In this thesis, the main goal is to correct the misalignment between the repeated studies.

3.4 Transmission - Emission Misalignment

The advantage of PET measurement is the accurate measurement of the absolute radioactivity concentration, made possible by methods to perform accurate attenuation correction, together with the nature of positron annihilation. In the thorax, the body attenuation is non-uniform and constant attenuation factors cannot be used. The attenuation has been corrected using transmission scanning [10]. Today, the PET cameras are combined with a CT camera, which can also be used for attenuation correction [49]. However, the attenuation scan cannot be acquired at the same time as the emission image, and this may lead to misalignment of the scans. The attenuation scanning is usually performed before emission acquisitions, and if patient movement occurs during the emission or between the rest and stress studies, the wrong correction may lead to errors

in the final images and quantitative values.

A lot of studies have been done to show the errors introduced by this misalignment, both for the transmission [3, 14, 69, 109] and for CT-based methods [49, 54, 60, 68]. When using the CT-based attenuation correction the problem is also the different time resolution [15,54,68] of PET and CT. The CT scan can be acquired with breath-holding as the PET scan is usually performed over many breathing cycles. It has been shown that the misregistration causes artificial defects in the anterolateral or lateral wall, which do not correspond to any typical territories of coronary distribution [60]. With most of the PET studies it is easy to visually assess the misplacement by overlaying the attenuation and emission scans, and then manually correct the misalignment. However, with O-15-labeled water studies, the problem is the poor contrast in emission images making it difficult to see this misplacement. In addition, it is rather time-consuming to visually analyze the whole dynamic image sets for every individual study.

Chapter 4

Simulation of Cardiac PET Data

PET is an *in vivo* method to study biological processes in a living body. The challenges in developing and improving image processing and analysis methods is that the reference values, the golden standards, are not available in real human data on which to base the comparison. The developed methods can provide more accurate diagnostic results, shorter computation time, and a possibility for better visualization [48]. The evaluation of the new method is usually performed using either physical or numerical phantoms and simulations. In addition, validations with animal experiments are used.

Physical phantoms are especially utilized for validation of the acquisition system and noise, along with reconstruction and analysis methods. The main limitation with physical phantoms is the difficulty to build realistic models of the organ motions and to simulate the dynamic biological behavior of the tissues. The construction of the numerical data consists of realistic simulations of the acquisition system, the patient anatomy, and the physiology of the tissues. The simulation of cardiac data should also include simulation of the heart movement. One of the main goals of the thesis is to construct realistic dynamic cardiac O-15-labeled water data for the evaluations. In this chapter, the different methods for the numerical simulation of the anatomy, movement, and physiology of the heart, and the PET measurement system are reviewed.

4.1 Simulation of Anatomy and Movement of Heart

The anatomy can be modeled by analytical or voxel-based phantoms. The analytical phantoms describe the shape and motions of the heart very realistically using mathematical functions. The simplest analytical phantoms are based on basic geometrical shapes, like ellipsoids [Publication I] or cones [5]. However, more realistic phantoms have been developed to also model the cardiac and respiration motions in the thorax, [78, 79, 87, 88]. The voxel based phantoms are described in 3D matrices, where every voxel is labeled according to the tissue the voxel belongs to. The segmentation of the 3D distribution of the tissues is usually done from high resolution anatomical images obtained with CT or MRI. Popular voxel-based phantoms for the brain are the

Hoffman brain phantom [36] and the Zubal phantom [113]. The voxel based phantoms are well suited to the human anatomy, but when the anatomy and spatial resolution are fixed, the simulation of biological variations and heart movement is difficult.

By using the knowledge about the motion of the heart and respiration obtained with high resolution imaging techniques, good models of the heart motion can be constructed. The MCAT (Mathematical Cardiac Torso Phantom) phantom is an example of a geometry-based phantom, which uses simple geometrical shapes (e.g. ellipsoids and cylinders) to model the heart and other organs in the thorax [78, 79, 88]. It includes both heart and respiration motions, and it can be used directly to simulate the emission and attenuation maps for gated SPECT studies. The advantage of the MCAT phantom is that it can be defined at any spatial resolution, and the anatomy and motions can be altered. In addition, the phantom can be used to model defects in the myocardium and a simple abnormal motion, mainly reduced ejection fraction. The NCAT (NURBS-based Cardiac Torso Phantom) phantom was developed to achieve more accurate and flexible representation of the human torso [87]. It uses non-uniform rational b-lines, so called NURBS surfaces. The model of the organs is based on CT data, and the heart motion parameters are derived from tagged MRI images. Recently, the NCAT phantom has been extended to include abnormal heart motion, by using finite-element models [100]. The new model of the motion has a more physiological background, and it can be used to model a variety of motion effects caused by the ischemic myocardium.

4.2 Simulation of Perfusion

To simulate the time-dependent behavior of tracer in the tissues, same principals that are used in the quantification can be used (section 2.2.2). In PET studies with O-15-labeled water, the behavior of the tracer can be modeled with a one-tissue compartment model. For the simulation of an input function for the LV, blood flow values for different tissues, values for the partition and extraction coefficient of the water, and the vascular volume of the tissue are needed. By averaging the measured arterial curves from real samples and fitting them to the rational or exponential function, good virtual TAC for the input, LV, can be constructed. The input curve can be also constructed using the TACs derived from the dynamic images. When using the measured arterial curve it needs be to taken into account that it is dispersed in the sample tubing, and the arrival times to the ROI, and to the sampling point, may be different [43, 99]. The distortion of the TAC is caused by smearing (dispersion) of the tracer bolus in the vessels due to inhomogenous velocity fields. Thus the input curve need to be corrected for time delay and dispersion. Similarly, there exists dispersion between TACs in the right ventricle (RV) and LV, because the blood circulates from RV to LV through the lungs. For this reason, another correction of the delay and dispersion needs to be done to construct a RV TAC. The Virtual TACs for the different structures can then be simulated by using the constructed input TAC and the desired values of the blood flow in the tissues.

4.3 Simulation of PET Acquisition

The PET measurement can be simulated numerically by use of analytical or Monte Carlo-based methods. The analytical methods are based on simple models of true measurements, especially on the noise in the sinogram. The positron emission follows the Poisson process, but after the corrections made to the raw data, the final data no longer follow the Poisson distribution exactly [30]. The MCAT and NCAT phantom simulators can be used to analytically simulate 3D distributions of the attenuation coefficient for a given photon energy, and distribution of emission radionuclide activity for the various organs [87]. The attenuation coefficients are derived from the known values of the coefficient of specific tissue, as the emission distributions are generated from the known uptake ratios of the specific radiopharmaceutical in the organs. The disadvantage of using analytical methods for the simulation of the PET measurement system is the lack of accuracy compared to the reality, but the method provides the possibility to produce large amounts of test data quickly.

Due to the development of powerful computers, the Monte Carlo-based methods have became popular in nuclear medicine [17, 111]. The Monte Carlo techniques are based on random variable sampling using numerical calculation methods. The Monte Carlo-based simulation models account for most of the phenomena encountered during the PET acquisition, like the Poisson nature of the emission, the positron range in tissues, the annihilation photons non-collinearity, scatter, randoms and system dead-time. This provides the possibility of more realistic simulations of the PET acquisition than with analytical methods. All the techniques have some common features, like a random number generator, rules to sample probability distributions, and sets of probability functions [111]. The choice of the simulator is based on the application to be used, and the desired accuracy, flexibility, efficacy and ease of use [17].

When simulating dynamic cardiac PET data, the simulator should enable the simulation of dynamic behavior of a specific PET tracer, and enable the simulation of organ and patient movements during the acquisition. Only two simulators have been designed so that the time-dependent behavior of the tracer can be easily simulated, PET-SORTEO and GATE [18]. The GATE simulator can also be used with moving anatomy [25]. The other important feature in the choice of the simulator is the computation time, as the main problem of Monte Carlo simulations has been the required computation time. When we need as many realizations as possible of the measurement with biological variation, the computation time becomes important. PET-SORTEO has been shown to be the most efficient simulator [81], although there is also increasing interest in and development of parallelizing other simulator codes [18]. In this thesis, the PET-SORTEO simulator was used, because it provides the possibility to simulate the dynamic behavior of the O-15-labeled water, and the computation time was short enough to perform many simulations for the evaluation of the developed methods.

Chapter 5

Alignment of Cardiac Structures in $[^{15}O]H_2O$ Perfusion PET studies

Alignment is a process which tries to find a mapping, a suitable spatial transformation, between two images. The alignment of medical images can be used to assist diagnostic decisions, monitor effects of therapy, or investigate the effects of intervention. The alignment process is often called registration, which is a step to find the alignment parameters between two or more images. The challenge in cardiac image registration is the mixed nonrigid motion of the heart and other thorax structures. In addition, compared to the brain images, there are no such anatomical landmarks in the cardiac images, which could be utilized in the registration.

Many methods have been developed for registration [39, 65] and a comprehensive review of existing cardiac registration methods is given in [67]. The choice of the registration method is based on the following; the application, what kind of features can be used (intensity values, surfaces, landmarks), what is the search space (rigid, affine, elastic), how to optimize the search for the alignment parameters, and what kind of metric is used to find the optimal result in the selected feature space. No general automatic alignment method exists to be used for different applications and data.

In this chapter, the alignment methods, which can be used with cardiac PET data, are briefly introduced. In this thesis, a novel approach to align 3D cardiac structures in O-15-labeled water PET emission images is developed and is described. Because the contrast is poor in O-15-labeled water cardiac PET images and no heart structures can be detected in time frame images, first the cardiac structures need to be extracted from dynamic images. The developed and studied methods for extraction of cardiac structures are also briefly introduced in this chapter. In addition, the method to automatically segment the volumes of interest (VOIs) for quantitative analysis in introduced.

5.1 Alignment of Cardiac Images

The heart movement due to the contraction of the heart, respiration and possible patient movement, is a real challenge for registration. In cardiac imaging, the registration can be used to correct the movement effects, or to align studies for comparison. External skin markers are not applicable in cardiac image registration since the registration of these landmarks does not guarantee the registration of the heart within the body. Also the body surface and lung surfaces have been proposed to be used in the registration. As with the external skin markers, the problem is the movement of the heart due to respiration and heart contraction. For these reasons, the best choice is the use of heart structures in the registration, producing better registration of the area of interest [66].

The image modality, available time and spatial resolution, as well as the objective of the registration, determine the choice of the search space of the image registration algorithm. With MRI it is possible to study the motion of the heart, due to the good spatial and time resolution, as well as the good contrast of the heart structures, the myocardium and ventricles, in the images. To register the heart structures from the different phases of the cardiac cycle, elastic registration, which can map lines onto curves [65], is needed to define the spatial relationship of the images. With dynamic PET images, where the shortest time frames are longer than one cardiac cycle, only the average heart shape can be detected. In the alignment of dynamic frame images, or dynamic studies, the rigid or affine registration can be used. Rigid registration in 3D is composed of 3 translation and 3 rotation parameters as the affine is composed of 9 parameters, also including the scaling, or 12 parameters, also including sharing in all dimensions.

The alignment of multimodality images brings complementary information for the diagnoses as the alignment of one modality images can be used in the comparison of the rest and stress images, to study the effects therapy, and the causes of intervention for the studied metabolism or function. In this thesis, the concentration is on the alignment of cardiac emission tomography images. External skin markers and optical tracking have been proposed to solve the registration of misaligned time frame images, caused by patient movement [70] [103]. As described above, the disadvantage of external methods is that knowledge of the heart position is missing, and the correction may lead to misregistration of the heart region. Attenuation scans have also been proposed to align the cardiac PET images, either using thorax surfaces [74] or correlation of intensity values [6]. The problem in this approach is the possible misalignment between the emission and transmission image. Moreover, because the heart structures cannot be detected from the transmission image, the registration does not lead to the best match of different heart structures. Methods which use the heart surface or intensity values of the emission image have been designed for both static SPECT images [24, 91, 92] and PET images [51, 98]. In [51] a registration method to compensate for the cardiac motion in a gated FDG study was developed, and in [98] an alignment method to correct the motion of dynamic N-13-labeled ammonia cardiac PET images was presented.

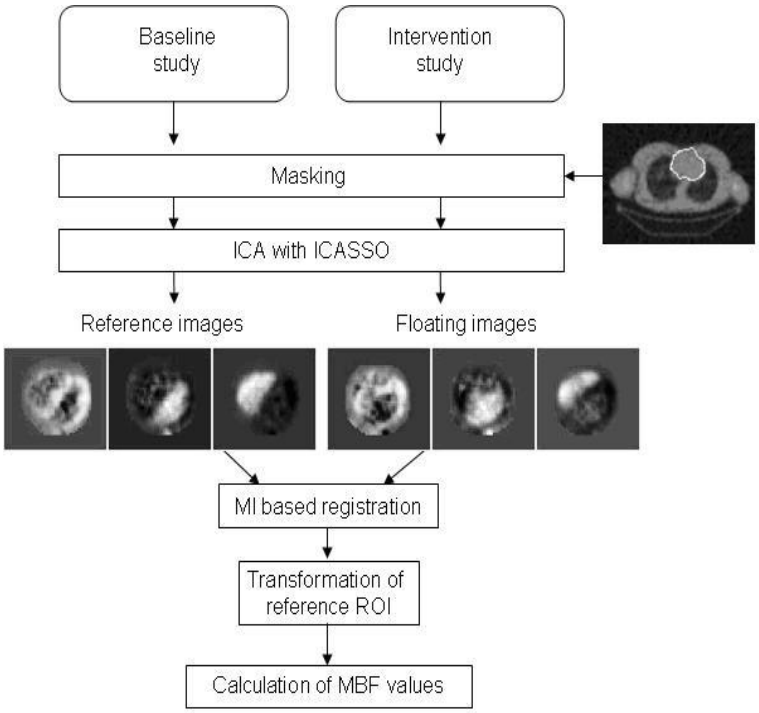

Figure 5.1: Schematic representation of the developed approach to align two dynamic studies.

5.2 Developed and Evaluated Methods Applied to Segmentation and Alignment of Cardiac Structures

There are no studies to align O-15-labeled water cardiac PET image sets. The challenge is the low contrast compared to the static SPECT images, or FDG PET images and for this reason the existing registration methods cannot be directly applied. In this thesis, a novel approach to align 3D dynamic O-15-labeled water cardiac PET images was developed and evaluated [Publications IV,V]. First, the cardiac structures are separated with independent component analysis (ICA) using the time-dependent behavior of the tracer in different tissues, and second, this separation result of the cardiac structures is used for the alignment of two image sets (Fig.5.1) [Publications I,III,IV,V]. Before the ICA method is applied to the dynamic $[^{15}O]H_2O$ emission data, the cardiac region is restricted using a segmentation algorithm developed in this theses [Publication II].

The final goal is to improve the quantification of the perfusion and decrease the variability of the results due the manual phases in the analysis. The alignment enables the use of the same ROIs for the quantitative analysis of the perfusion values in the intervention studies. The ROIs for the quantitative analysis can be derived from the

reference study either manually [Publication IV] or automatically [Publications I,V]. The competing strategy for the alignment would be to automatically segment the ROIs from the intervention studies without alignment [Publication V].

5.2.1 Segmentation of Cardiac Structures

Segmentation is a process that separates objects in an image. The automatic segmentation of PET images is a challenging task, because the images are usually noisy compared to their contrast. The segmentation can be performed manually, like traditionally the ROIs have been defined [Publications III,IV]. However, the problem is the large amount of data to be segmented in 3D or even 4D, which is difficult to perform manually, and is a time-consuming process. The results are also dependent on the observer. Furthermore, the results may vary between different observers (inter-observer variability), and also differ on different days with the same observer (intra-observer variability), resulting in decreased reproducibility of the results. In this thesis, a new method to extract the heart region from the PET transmission images was developed. In addition, the ICA separation of the cardiac structures from dynamic $[^{15}O]H_2O$ PET data was evaluated. For the extraction of the ROIs with human data, a manual approach was used. Preliminary tests to automatically extract the volumes of cardiac structures from simulated data were also performed in this study.

Segmentation of PET Transmission Images for Heart Volume Extraction

A transmission measurement is performed to compensate for the effect of the attenuation of annihilation photons in the subject's body. The contrast between soft tissue and lungs is high in transmission images compared to the emission images. Because of this, the transmission images have been used for motion detection and correction [7]. The segmentation of the transmission images has also been used to calculate more accurate attenuation factors [2, 108, 110]. In this thesis, the transmission image was used to produce a rough heart region mask. The mask is used to restrict the emission image, so that the assumption of the number of components in the ICA model becomes more valid, and also the restriction of the data decreases the computation time. In addition, the liver is problematic for the ICA separation, because its functional behaviour is similar to that of the myocardium. With the anatomical heart volume mask it can be eliminated from the ICA separation. First, the transmission image is segmented to soft tissue, lungs and background, and second, the segmentation result is used to extract the heart region as seen in the transmission image [Publication II]. The segmentation was based on the Markov Random fields [13], and the heart region was extracted using the DM-DSM (Deformable Models with Dual Surface Minimization) surface extraction algorithm [50, 97]. Because of the possible movement between the emission and transmission scanning, the obtained mask was enlarged to ensure that the whole heart was inside the mask during the dynamic emission image.

Separation of Cardiac Structures from Dynamic $[^{15}O]H_2O$ Cardiac PET Data

The challenge of dynamic O-15-labeled water images is the low contrast between the tissues. The radiopharmaceutical is at the beginning mainly present in the blood pools and at the end of the study also in tissues like the liver and the myocardium [8]. This makes it difficult to extract the different tissues automatically from individual time frame images. However, the separation of cardiac structures from dynamic images can be performed utilizing the time-dependent behavior of the tracer in the tissues. ICA [41] is a method which uses this information and has shown its capability to separate cardiac structures from dynamic data [55–57, 63, 64] [Publication I,III,IV,V]. For this reason, we used the ICA method for the separation.

The advantage of using ICA is that no additional scan for the blood pool is needed [10], only the number of components needs to be defined in advance. The results of the separation are component images, which are showing the most probable position of the different structures in the dynamic scan [Publication III]. Therefore, it was assumed that only a little or no patient movement occurs during the acquisition. To solve the ICA model in dynamic cardiac PET data, the FastICA algorithm was used [40]. The choice was based on the fast computation time of the algorithm. To obtain a valid guess of the number of the components, the image space was restricted [Publications I,III,IV,V]. The construction of the mask is described in more detail above.

Automatic Volume Extraction of Cardiac Structures

To quantify the myocardial perfusion, the TACs for the arterial blood pool and the myocardial tissue are measured from the dynamic image. The TACs are derived from the ROIs or VOIs, which defines the region or volume of the myocardium and LV. Conventionally, the ROIs are drawn manually to the differential images. The differential images are constructed by the subtraction of the first time-frame images from the last time-frame images to enhance the contrast of the myocardium. In this thesis, the manually derived ROIs were used to evaluate the developed alignment method with human data. Because the construction of the differential images is subjective, we tested to improve the ROI drawing by the use of ICA separation result images instead of the differential images [Publications III,IV]. The good contrast of the cardiac structures in the ICA separation images also provided the possibility to automatically derive the VOIs for the quantitative analysis. For the automatic segmentation of the VOIs, the same surface extraction method, which was used for the extraction of the heart volume from the transmission image, was tested in this thesis with simulated data [Publications I,V] [50, 97].

5.2.2 Alignment of 3D Cardiac Structures in $[^{15}O]H_2O$ PET Emission Images with Mutual Information

To align the ICA component images, a second segmentation could be performed to extract the surfaces of the separated cardiac structures for surface-based registration, or use the segmented component images directly with intensity-based registration. The segmentation of the myocardium is difficult, and the extraction of the surface is demanding, especially from stress images, because of the cardiac movements, spillover and partial volume effect. For this reason a normalized mutual information (NMI) based method for the alignment was chosen [Publications IV,V].

Mutual information (MI) based registration methods have shown promising results, especially in multimodal registration [1, 101], and have been used in many clinical applications [77]. MI is an information theory based measure of the statistical dependence between two random variables [62, 105]. In other words, mutual information measures how much one image describes the other, and assumes that when these two images are perfectly aligned, one image provides the most information about the other. The advantage of MI is that only few assumptions are made regarding the nature of the relation between the image intensities. Mutual information can be defined as

$$MI(A, B) = H(A) + H(B) - H(A, B), \tag{5.1}$$

where $H(A)$ and $H(B)$ are entropies of the images A and B, and $H(A, B)$ is the joint entropy of these images. This means that the mutual information is maximized when the joint entropy of the images A and B is minimized. The problem is that the joint entropy can be really low even when the images are totally misregistered. For this reason, NMI was proposed [94], which is less sensitive to changes in overlap:

$$NMI(A, B) = \frac{H(A) + H(B)}{H(A, B)}. \tag{5.2}$$

The joint entropy distribution of intensities in two images can be estimated from a joint histogram of intensities [77]. Each entry $h(a, b)$ in the histogram denotes the number of times intensity a in one image coincides with b in the other image. The probability distribution is the division of the entries by the total number of entries. By summing over the rows and columns the probability distribution for the each image can be estimated.

Based on the ICA theory [41], there is no way to retain the magnitudes of the original intensities in the segmentation, and for this reason it is important that the similarity measure is not dependent on the actual intensity values. It was assumed that there would be only rigid registration between the image sets, because the image sets to be aligned were from the same subject, and the dynamic frame images were assumed to represent the average position and orientation of the heart motion. Additionally, the 9 parameter affine registration was tested [Publication IV]. The novel idea in the developed approach is also that not all cardiac structures need to be used in the alignment.

It was tested using only the RV, both ventricles and all three structures for the alignment. The idea is that if the myocardium is not well segmented or the shape has been deformed due to a disease, like in ischemic dilation, the ventricles alone could be used for the alignment. When using more than one structure in the registration algorithm, the histogram to be used for the NMI calculation was constructed using voxels from all structures. To avoid possible interpolation errors in the final quantitative values, the found transformation parameters were applied to the ROIs drawn on the reference image instead of reslicing the original dynamic images.

Chapter 6

Experiments and Results

In this chapter the evaluation results of the developed and evaluated methods are summarized. In addition, the construction of the simulation data is described, and the human data used for the evaluations is presented.

6.1 Simulated Data in this Work

The simulation of realistic dynamic cardiac O-15-labeled water data was composed of the simulation of the physiology, anatomy, and movement of the heart, and the realistic simulation of the measurement system. In [Publications I,IV,V] different simulations were carried out, and the simulated data are now briefly described.

Two different anatomies were used in the simulations; simple 2D representation of the thorax [Publication I], and 3D MCAT based anatomy [Publications I,IV,V] (Fig. 6.1). In addition, normal heart and respiration motion was included in the simulation process [Publications I,V]. Because, in the PET-SORTEO simulator, it was not possible to include moving anatomy in the simulations, we needed to construct the movement into the static 3D anatomical volume. The motion was included in the simulation in two

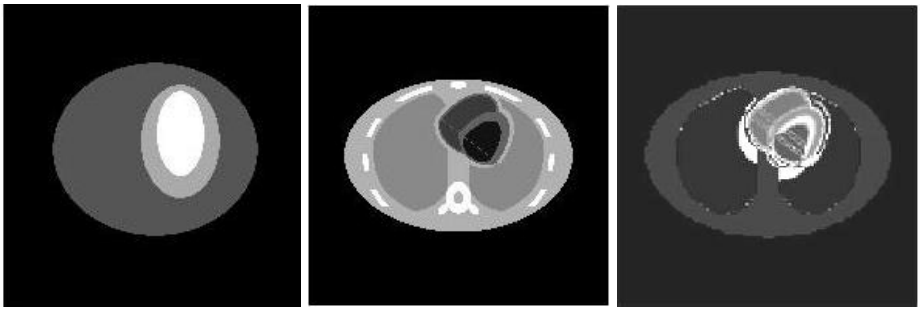

Figure 6.1: Example of transaxial slices of the anatomical phantoms used for the simulations: 2D phantom (left), 3D MCAT phantom (middle), 3D MCAT motion phantom (right).

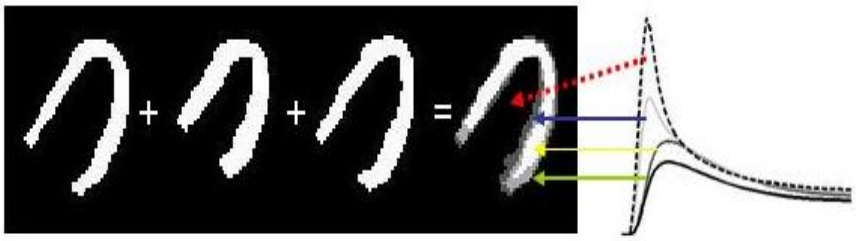

Figure 6.2: An example of the construction of the motion phantom in [Publication V]. Different time phases over cardiac and respiratory cycle were summed together and averaged. The anatomical volume was labeled according to the fraction of the tissue present in a voxel. The TAC for that voxel was averaged from the pure tissue TAC of the tissues present in the voxel.

different ways. In [Publication I], the study was constructed so that we had at the same time cardiac and respiratory gated time-frames with dynamic behavior of the tracer, meaning that every time frame image was simulated separately with different anatomy. In [Publication V], the motion was averaged over four time phases of the cardiac and respiratory cycles, and the final phantom image was labeled on the basis of the fraction of the tissues present in one voxel over time (Fig. 6.2). In [Publication V] also one case with a hypoperfused region was simulated.

The TACs for the tissues were simulated on the basis of the one-tissue compartment model of the O-15-labeled water. The input, the LV curve, was generated by correcting the delay and dispersion from the measured arterial sampled blood TACs and then fitting them to the rational function [Publications I,IV,V]. In [Publications IV,V] also the right ventricle TAC was simulated by removing the dispersion from the left ventricle curve and moving the curve 10 seconds towards the start of the scan. By changing the flow values, different conditions (rest and stress) of the myocardium, and also the time-dependent behavior of the other tissues (body, lungs, liver) were simulated (Fig. 6.3).

Both analytical and Monte Carlo simulations were used to simulate the PET acquisition. The analytical method was based on [30], and the noise was added to the sinogram bins before reconstruction [Publication I]. The Monte Carlo simulations were based on the PET-SORTEO simulator [81,82]. The reconstruction of the sinogram data was performed with the use of the ordered-subsets expectation maximization (OSEM) algorithm [Publication IV] and the filtered back projection (FBP) algorithm [Publications I,V].

6.2 Human Data in this Work

The PET data were acquired with a GE Advance scanner (General Electric Medical Systems, Milwaukee, Wisconsin, USA) at the Turku PET centre from healthy fe-

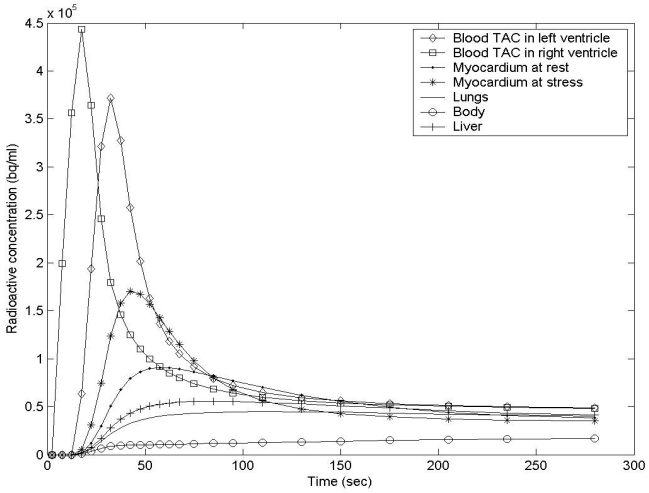

Figure 6.3: Simulated TACs used for the numerical phantom simulations.

male volunteers [Publications II,III,IV]. A transmission scan was acquired before an emission scan. For every positron emission tomography study, 700 to 900 Mbq of $[^{15}O]H_2O$ was injected over 20 seconds. The number of time frames collected was (14x5s, 3x10s, 3x20s and 4x30s). After a 10-minute period to allow for radioactivity decay, the adenosine infusion (140 μg/min/kg) was started, and a dynamic PET scan similar to that at rest was performed. The reconstruction of the sinogram data was performed by use of ordered-subsets expectation maximization (OSEM) algorithm [Publication III, IV].

The test data set for the segmentation of the transmission images consisted of 25 transmission images. The ICA separation was tested with 25 rest studies and 6 adenosine-induced stress studies. To evaluate the developed alignment method six rest-stress images sets and 10 rest-rest images acquired on different time occasions were used.

6.3 Evaluation of Results

To select one method over another is not an easy task. Visual analysis of the result has been shown to be a reliable method to detect even small inaccuracies in the image registration of brain PET images [106]. The visual evaluation can also be used with real patient data, but the results are dependent on the observer and it is an informal way to evaluate the results. With the simulated data, the accuracy of the results achieved with different methods can be quantified. The quantitative values of e.g. segmented volumes, shapes, different size measures, computation time, and the needed capacity

of computer power to run the algorithm, can be calculated. In the alignment approaches the found alignment parameters can also be compared to the ground truth values. However, the difficulty is to distinguish errors of translation from rotations, and the accuracy of the results may vary in different locations of the images in 3D [107]. The mean and root-mean-square errors in different locations of the image are also commonly used to assess the accuracy of the alignment [67].

The accuracy of the alignment results was tested by comparing the similarity of the aligned volumes to the ground truth volumes with a volume similarity measure, the Jaccard coefficient [46,47] [Publications I,II,IV,V]. It is defined as $|A \cap B|/|A \cup B|$ and it measures the similarity of two binary volumes (A and B) in the scale from 0 to 1. This means that if the coefficient gets the value 0, the two volumes do not share any common voxels in 3D space and similarly, if the coefficient gets the value 1, the two volumes are identical. The coefficient with simulated data was also used to compare image segmentation and registration-based methods for analyzing misaligned dynamic image sets [Publication V], similarly as we have proposed to be done with brain images [96]. The volume measure provided the possibility to compare the two different methods with each other. In addition, the Jaccard coefficient was used to evaluate the accuracy of the ICA separation result in [Publication I].

The final goal is to improve the quantitative analysis of the perfusion studies and decrease the variability of the results due to the manual phases. For this reason, the perfusion values were also calculated with real human studies. The results were compared to values obtained with traditional manual methods [Publications III,IV]. When working with real human data, where the ground truth values are not know, the comparison of the methods provides an answer to the question of whether the two methods perform similarly or not. It can also give information about the variances in the results. In [Publications III,IV] we assumed that the manual definition of the ROIs gave us the ground truth about the perfusion values. Additionally, visual evaluation of the results were performed in all studies.

6.4 Results

Segmentation of PET Transmission Images for Heart Volume Extraction

An example of a visual result of the segmentation and extracted heart region mask is shown in Figure 6.4. The segmentation of the transmission images were excellent in all cases in visual inspection. The automatically extracted heart volumes covered the whole heart region, but in some cases the volume also covered the chest wall. The extracted anatomical heart volume mask provided the possibility to eliminate most of the liver tissue from the ICA separation.

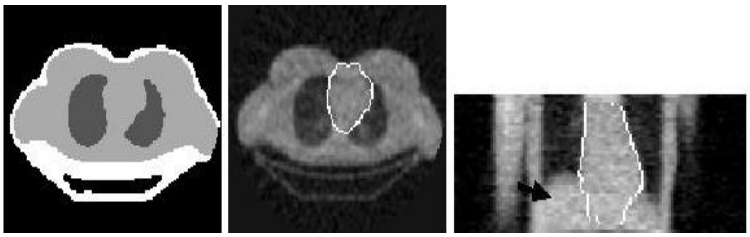

Figure 6.4: An example of the segmentation of PET transmission image and the extracted heart region mask. The black arrow is pointing to the liver.

Separation of Cardiac Structures from Dynamic $[^{15}O]H_2O$ Cardiac PET Data

On visual inspection, the different cardiac structures were well separated with ICA in all test cases with the simulated and human data [Publications I,III,IV,V]. A typical example of the separation of the cardiac structures from the human data is shown in Figure 6.5. For comparison, the corresponding conventional differential image is shown. Clearly, the cardiac structures are better visualized in the ICA separated component images in the differential images [Publication III] (Fig. 6.5). In Monte Carlo-simulated phantom data, the separation of the myocardium was not optimal, but the challenge of this data was the really high noise compared to the resolution [Publications I,IV,V].

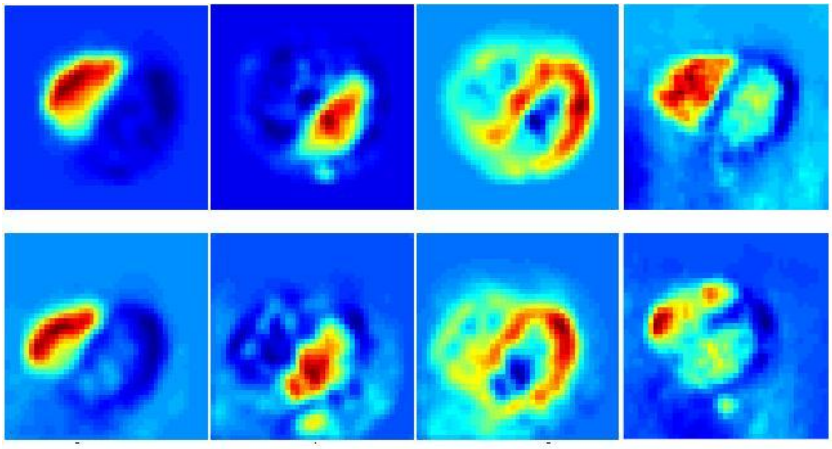

Figure 6.5: An example of the ICA separation of the cardiac structures from O-15-labeled water images with human data (left to right: RV, LV, myocardium), transaxial slices from the rest study (top) and from the stress study (bottom). For comparison, the manually defined differential images for corresponding studies (right).

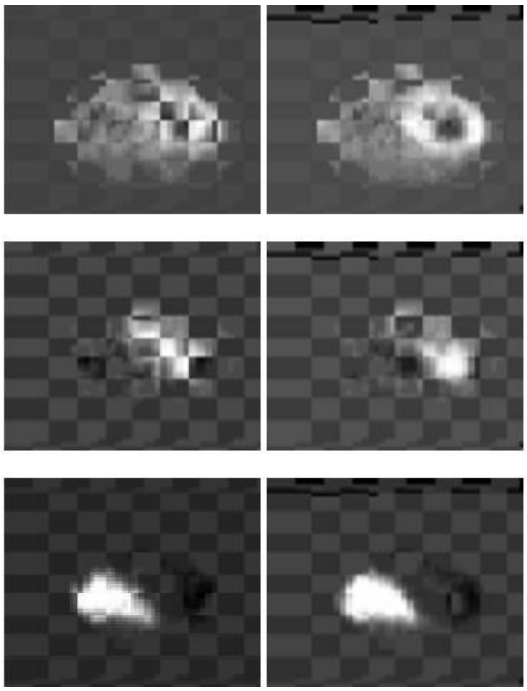

Figure 6.6: Visual result of the alignment with the human data. The two component images are overlaid so that every other box is from the other image, (left) before the alignment and (right) after the alignment.

Alignment of Cardiac Structures in $[^{15}O]H_2O$ PET Emission Images with Mutual Information

Examples of the visual result of the alignment for the simulated phantom data and human data are given in Figures 6.7 and 6.6. The perfusion values calculated using automatically aligned ROIs were found to be similar to the values calculated using conventional method [Publication IV]. The phantom results showed that the developed method is excellent in the alignment of translational misalignments, but with rotational movement the results were not as good. The reason for this could be the small amount of information about the rotation in the ICA-separated images. In [Publication IV], it was found that the alignment performed well with different anatomies, including one simulated ischemic heart case. It was also found that the alignment could be done without the use of information from the myocardial compartment. The rigid and affine registration yielded similar results.

The alignment of the studies decreases the total analysis time and the manual phases in the analysis, thus improving the repeatability of the results. In addition, the alignment can assist the visual analysis of the studies (Fig. 6.8). The visual comparison of equivalent myocardial segments is easier when the corresponding transaxial slices are

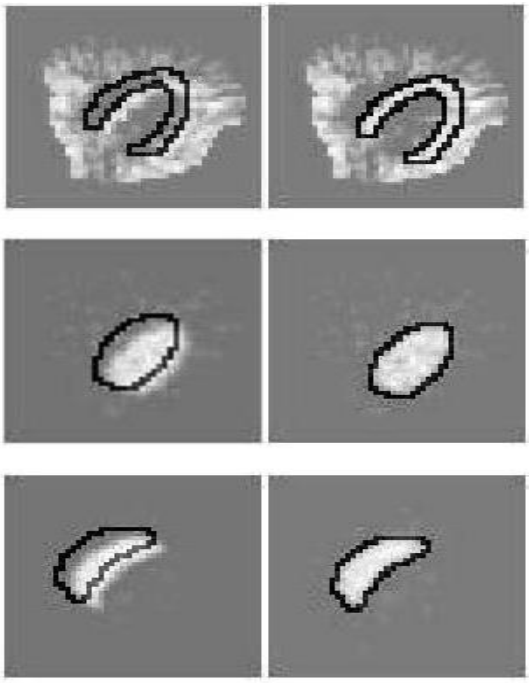

Figure 6.7: Visual result of the alignment with the simulated phantom data, the ROIs before the alignment (left) and after the alignment (right).

showing the same anatomical regions.

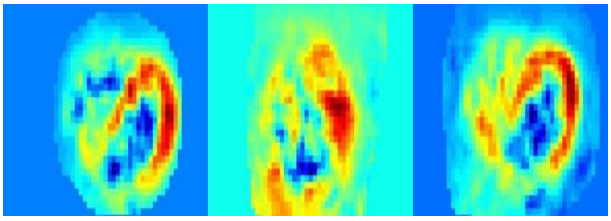

Figure 6.8: ICA component images of the myocardium from the same transaxial slices of the reference study (left), the floating study before the alignment (middle), and the floating study after the alignment (right).

Automatic Volume Extraction of Cardiac Structures

The automatic extraction of the ventricle volumes for quantitative analysis from ICA-separated images was tested with simulated data [Publications I,V]. As mentioned above the separation result of the myocardium was not optimal with the simulated

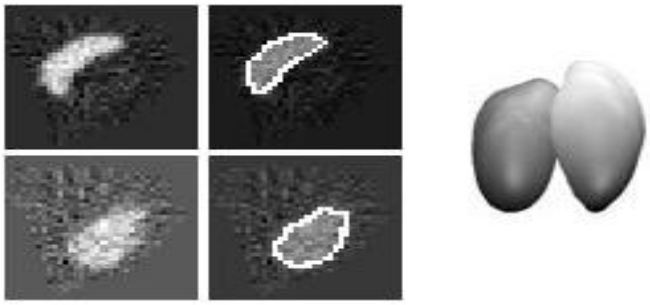

Figure 6.9: An example of the automatically extracted ventricle volumes with simulated data, (left) ICA component image of the RV (top) and LV (bottom), the extracted surfaces for the RV and LV (middle), and the 3D visualization of the extracted volumes (right).

data and for this reason the myocardial component was not used for the automatic volume extraction. Visually, the volumes of the ventricles were extracted well (Fig. 6.9) [Publications I,V]. The quantitative evaluation also supported the good correspondence between the extracted volumes and the true volumes of the ventricles [Publication I,V].

Chapter 7

Discussion

In this thesis, a novel process to align $[^{15}O]H_2O$ perfusion PET studies using cardiac structures was developed. To separate the cardiac structures from $[^{15}O]H_2O$ perfusion PET studies, the ICA method was evaluated. In addition, to quantitatively evaluate the developed approach, realistic simulated data was constructed.

In clinical and research use, reliability and accuracy of the images processing method has to be confirmed before using the method. The evaluation can be done using simulated data. There are publicly available data bases of simulated brain PET data, which researchers can use to evaluate their methods [81]. Such data bases were not available for cardiac perfusion PET studies, and for this reason there was a need to construct realistic data for the evaluations. Because there were no publications, in which realistic numerical cardiac PET data were constructed, the simulations were started with simple 2D representation of the anatomy and analytical model of the PET measurement [Publication I]. The simulation process was made more realistic during the thesis, and the last version of the simulated data also included the cardiac and respiration motion with the dynamic behavior of tracer by using the realistic Monte Carlo-based simulator [Publication V]. Once the evaluation of the simulated data against the real data has been made, it can be made publicly available.

A great challenge in the cardiac region is to realistically simulate the functional and anatomical features of the heart. Until now, only one report has been recently presented, where both have been taken into account during the simulation of PET acquisition [25]. The problem is the complexity of the simulation and time required to perform it. Because, with PET-SORTEO it was not possible to use moving anatomy, a novel idea to construct the anatomical volume so that the cardiac movements were included in the static 3D anatomy was developed [Publication V]. However, to make the simulation more realistic also the movement between the time frames should be considered.

The O-15-labeled water in the myocardium can be modeled with a simple one-tissue compartment model. It was found that the real challenge is to realistically model the physiological behavior of the other tissues in the thorax region, as in the lungs and liver. The lungs contain a lot of air and vessels which have a high radio activity concen-

tration in the blood. Because of this, the homogenous model of the lungs, which was available in the MCAT phantom, is not realistic enough. The problem in simulating the time-dependent behavior of the liver, is that only part of the blood input is coming through the arterial side; most of the blood is flowing form the portal side. In our simulations, only the arterial side was taken into account, and for this reason the simulated perfusion in the liver is lower than in the real studies.

Simulations, however, are only models of reality. For this reason it is important to test the developed methods with real human data. In this thesis, the developed approach was also tested with human studies from healthy subjects at rest (25 studies) and at pharmacological stress (6 studies). However, more extensive tests and evaluations with real patient data need to be done, to show the feasibility of the methods for wider use in drug development and clinical diagnostics. In addition, it would be interesting to test the alignment method in a real drug study, and evaluate qualitatively the effect of the alignment on the reproducibility of the results.

O-15-labeled water is an attractive tracer, because of its short physical half-life and because its kinetics permits accurate quantification of the myocardial perfusion in absolute terms. However, the disadvantage has traditionally been the low contrast between the tissues. In this thesis, ICA was applied to separate the cardiac structures from the dynamic study. It was found that the method is capable of automatically and reliably separating the ventricles and the myocardium with different blood flow levels [Publication I], at rest and at pharmacological stress [Publications III,IV], under cardiac and respiration motion [Publications I,V], and patient movement [Publications IV,V]. However, patient movement during the study could affect the ICA separation. In [80] it was shown that the movement in the beginning of the study, where the activity is high in the ventricles, affected the separation result more than the movement in the later time frames. The high noise also affects the ICA separation [64], as was seen in the phantom data results. The separation of the myocardium was better with real human data [Publications III,IV] than by using the Monte-Carlo simulated phantom data. The reason for this could be that the simulation was based on the technical parameters of a PET scanner designed for brain studies, and not commonly used for cardiac imaging.

To better meet the prior assumption of having a certain amount of independent components, the image space was restricted by masking out the regions which did not include the heart. In this thesis, a new method to construct the mask automatically using transmission images was developed [Publication II]. Earlier the mask has been defined manually [57]. Due to the nature of the transmission images, the exact heart volume cannot be extracted, only a rough region where the heart is located. The problem in using transmission images to localize the heart is also the possible misalignment of the emission and transmission scans. However, it was found that the extracted mask was applicable to spatially restrict the emission image for the ICA segmentation process.

The quantitative and visual results proved that the developed alignment approach finds the misalignment between the image sets under rest and stress conditions [Publications IV,V]. Studies have been done to try to compensate for the movement in dy-

namic $[^{15}O]H_2O$ cardiac PET images [70, 103]. These methods are based on external markers or optical tracking, and the aim of the methods is to compensate the patient movement between the time-frame images. To use external motion tracking for the alignment of two studies would require that the studies are performed during the same day without detaching the markers. This is not practical when monitoring therapeutic or drug interventions over a long time period. The advantage of our method is that cardiac structures as seen in the emission images are used in the alignment that more accurately defines the position and orientation of the heart. For the registration phase, the intensity-based method was used. The idea was, at the beginning of the study to segment the surfaces of the cardiac structures for the alignment task [Publication I]. The problem of using the tissue surfaces is that one extra segmentation is needed, which increases the total time used for the registration.

In the developed approach, the movement during the dynamic study was not taken into account, because the contrast in the time-frame images is low, and it is extremely difficult to correct the movement between the time-frame images by using only the emission data. In addition, the transmission-emission misalignment was not corrected. However, we found translations of even 30 mm between the rest and stress image sets, which were corrected with the same attenuation scan. This affects the final quantification of the perfusion values, but we believe that the alignment of emission studies can be performed well even with this misalignment. Usually, the misalignment of emission and transmission affects especially the quantification of the perfusion values in the myocardium [3, 14], however, our approach performed well using only the RV structure in the alignment. In this way the possible abnormalities in the myocardium can be discarded in the alignment.

Using the alignment, the comparison of the studies can be done in equivalent myocardial segments using the same ROIs. This increases the accuracy and repeatability of the quantitative analysis. In addition, the visual comparison of the studies becomes easier when the corresponding transaxial slices are representing the same cardiac structures. Commonly, the cardiac data are re-orientated into the short axis image with semi-automatic methods, before calculating the regional perfusion values. Similarly, as by drawing the ROIs to the transaxial images, the variability of the results can be decreased by aligning the studies before re-orientation, because after alignment the same transformation parameters can be used to orient the data to short-axis images.

In [Publication IV] it was also suggested that instead of reslicing the original data, the ROIs are translated and rotated to avoid possible interpolation errors in the quantitative values. It has been shown that if the axial resolution is not good, the re-orientation may cause some errors in the final results [34]. To find out the real effect of the reslicing, further studies are needed.

In this thesis, it was shown that by using the cardiac structures extracted from the emission scan, two image sets can be aligned so that the same ROIs could be used. Nevertheless, the found information about the misalignment of ICA component images could also be used to correct the transmission-emission misalignment or align the O-

15-labeled water study to an anatomical image, like CT. In the future, the feasibility of these possibilities will be further investigated .

Manually defined ROIs were used for the quantitative analysis of human data, which were then aligned by using the proposed alignment approach. By use of volume extraction with deformable models, the 3D volumes of the ventricles were automatically extracted, which could then be used as a 3D ROI for the input function [Publications I,V]. The challenge is still to extract the surface of the whole myocardium from the component images. In the future, the idea is to automatically extract the ROIs from the baseline study and use them for the intervention study after the alignment.

7.1 Author's Contribution

The author designed the new approach to improve the analysis of the O-15-labeled water perfusion studies by alignment of cardiac structures and was responsible for the concatenation of the algorithms. However, all the publications included in this thesis are the result of a group effort. Especially, the ICA separation part was done in collaboration with M. Magadan-Mendez. This thesis is covering the evaluations of the ICA method to extract reliably the cardiac structures. As the first author of the [Publications I,II,IV,V], A. Juslin was responsible for the writing, and overall preparation of the publications. The author performed and designed all the simulations and evaluations in [Publications I,II,IV,V]. In [Publication II] the idea of using the transmission images for the construction of the mask for the ICA separation was originally the author's, as was the use of deformable models for the extraction of the heart surface. The author also participated in the implementation of the method. In [Publication III], as a second author, A. Juslin had an important and active role in designing and writing the publication. In addition, the masking of the data was performed by the author. In [Publication IV], specifically, the ideas of using different structures for the alignment and realignment of the ROIs were the author's.

7.2 Concluding Remarks

The quantification enables an objective and exact way to compare studies acquired on different time occasions, under different conditions, and with different subjects. To perform the visual and quantitative comparison of the studies, we need to ensure that the analysis is done in equivalent myocardial segments. In addition, because only a limited number of PET studies can be performed with humans, it is important that all the studies can be analyzed. In this thesis, a novel process to align $[^{15}O]H_2O$ cardiac perfusion studies was developed. The evaluation results proved that the developed approach can be used in practise with real human studies. The alignment provided the possibility to use the same ROIs for the repeated studies, which decreases the operator time needed for the analysis. The developed approach can facilitates the quantitative and visual

analysis of the studies. With the automatic image processing and analysis methods the variability of the results can be decreased and the repeatability and accuracy of the quantification increased.

Chapter 8

Summary of Publications

I A. Juslin, A. Reilhac, M. Magadan-Mendez, E. Alban, J. Tohka and U. Ruotsalainen, "Assessment of separation of functional components with ICA from dynamic cardiac perfusion PET phantom images for volumes extraction with deformable models," in *Third International Conference on Functional Imaging and Modeling of the Heart (FIMH'05)*, Lecture Notes of Computer Science, vol 3504, 2005, pp. 338–347.

The ICA method was tested for the separation of the cardiac structures with different blood flow levels of the myocardium in a simulation study. In addition, the effect of the motion of the heart, due to the cardiac contraction and respiration, was tested. For the evaluation realistic 2D and 3D phantom data were constructed. The visual results of the separation of cardiac structures were good with different flow levels and with motion, although the segmentation result of the myocardium was not optimal with motion phantom. The extraction of the ventricle volumes with deformable models was also demonstrated.

II A. Juslin, and J. Tohka, "Unsupervised segmentation of cardiac PET transmission images for automatic heart volume extraction," in *Proceedings of the 28th Annual International Conference of the IEEE Engineering in Medicine and Biology Society (EMBC'06)*, New York, USA, August 30 – September 3, 2006, pp. 1077–1080.

An automatic and unsupervised segmentation method to extract the rough heart region from the transmission image was developed. The obtained heart region can be used to mask the corresponding emission image, so that the heart region is only used for the further processing, like ICA separation. The method was tested with 25 patient images, and visual results were good in all cases.

III M. Magadan-Mendez, A. Juslin, SV. Nesterov, J. Knuuti, and U. Ruotsalainen, "Automatic ICA segmentation and Analysis of Dynamic $H_2^{15}O$ cardiac PET images," in *IEEE Transaction on Information Technology in Biomedicine*, submit-

ted, 2007.

The automatic ICA-based separation of the cardiac structures was introduced and tested with human data (25 rest studies and 6 pharmacological stress studies). The results were visually good in all cases, and showed that the cardiac structures can be extracted from real human data with ICA. The separation of cardiac structures also improves the positioning of the ROIs in the $[^{15}O]H_2O$ cardiac PET images.

IV A. Juslin, J. Lötjönen, SV. Nesterov, J. Knuuti, and U. Ruotsalainen,"Alignment of 3-dimensional cardiac structures in O-15 labeled water PET emission images with mutual information," *Journal of Nuclear Cardiology*, vol 14, no.1, 2007, pp. 82-91.

A novel approach to align two dynamic O-15-labeled water images was introduced. First, cardiac structures from the dynamic O-15-labeled water images are separated using ICA, and second, the resulting component images are aligned with the normalized mutual information-based registration. The developed approach was shown to be applicable for the alignment task with both simulated phantom data as human data with two different conditions (10 rest study pairs and 6 pharmacological stress study pairs). The alignment of the studies assists the visual analysis,and it may decrease the variation in the quantitative results.

V A. Juslin, J. Tohka, J. Lötjönen, and U. Ruotsalainen, "Comparison of image segmentation and registration based methods for analysis of misaligned dynamic $H_2^{15}O$ cardiac PET images ," in *Proceedings of the IEEE Medical Imaging Conference (MIC2006)*, San Diego, USA, December 1–4, 2006, pp. 3200-3204.

The developed alignment approach was further evaluated and compared to the image segmentation-based method to analyze misaligned dynamic $[^{15}]H_2O$ cardiac PET images. For the evaluation, simulated phantom data was constructed with different anatomies and perfusion levels. In addition, a novel way to include cardiac and respiratory motion in the simulation was developed. The alignment method was shown to be accurate to detect misalignment of two image sets. The results also showed that the segmentation-based approach was capable of extracting ventricle volumes well. In the future, the aim is to automatically extract the ROIs from the baseline study and use them for the intervention study after the alignment.

References

[1] U. Aladl, G. Hurwitz, D. Dey, D. Levin, M. Drangova, and P. Slomka, "Automated image registration of gated cardiac single-photon emission computed tomography and magnetic resonance imaging," *Journal of Magentic Resonance Imaging*, vol. 19, pp. 283 – 290, 2004.

[2] J. Anderson, R. Srinivasan, B. Mair, and J. Wotaw, "Hidden markov model based attenuation correction for positron emission tomography," *IEEE Transaction on Nuclear Science*, vol. 49, pp. 2103 – 2111, 2002.

[3] J. Andersson, B. Vagnhammar, and H. Schneider, "Accurate attenuation correction despite movement during PET imaging," *Journal of Nuclear Medicine*, vol. 36, pp. 670 – 678, 1995.

[4] L. Axel and L. Dougherty, "Heart wall motion: improved method of spatial modulation of magnetization for MR imaging," *Radiology*, vol. 172, pp. 349 – 350, 1989.

[5] H. Azhari, M. Buchalter, S. Sideman, E. Shapiro, and R. Beyar, "A conical model to describe the nonuniformity of the left ventricular twisting motion," *Annals of Biomedical Engineering*, vol. 20, pp. 149 – 165, 1992.

[6] S. Bacharach, M. Douglas, R. Carson, P. Kalkowski, N. Freedman, P. Perrone-Filardi, and R. Bonow, "Three-dimensional registration of cardiac positron emission tomography attenuation scans," *Journal of Nuclear Medicine*, vol. 34, no. 2, pp. 311 – 321, 1992.

[7] D. Bailey, "Transmission scanning in emission tomography," *European Journal of Nuclear Medicine*, vol. 25, no. 7, pp. 774 – 787, 1998.

[8] S. Bergmann, K. Fox, A. Rand, K. McElvany, M. Welch, J. Markham, and B. Sobel, "Quantification of regional myocardial blood flow in vivo with $H_2^{15}O$," *Circulation*, vol. 70, pp. 724 – 733, 1984.

[9] S. Bergmann, P. Herrero, J. Markham, C. Weinheimer, and M. Walsh, "Noninvasive quantification of myocardial blood flow in human subjects with oxygen-15-

labeled water and positron emission tomography," *Journal of American Collegue of Cardiology*, vol. 14, pp. 639 – 652, 1989.

[10] S. Bergmann and B. Sobel, *Positron Emission Tomography of the Heart*. Futura Publishing Company, Inc., 1992.

[11] D. Berman, R. Hachamovitch, L. Shaw, J. Friedman, S. Hayes, L. Thomson, and et al., "Roles of nuclear cardiology, cardiac computed tomography, and cardiac magnetic resonance: Nonivasive risk stratification and a conceptual framework for the selecting patient with known or suspected coronary artery disease," *Journal of Nuclear Medicine*, vol. 47, no. 7, pp. 1107 – 1118, 2006.

[12] R. Berne and M. Levy, *Cardiovascular Physiology*. Mosby, 1997.

[13] J. Besag, "On the statistical analysis of dirty pictures," *J R Stat Soc, Ser B*, vol. 48, no. 3, pp. 259 – 302, 1986.

[14] V. Bettinardi, M. Gillard, G. Lucignani, C. Landoni, G. Rizzo, G. Striano, and F. Fazio, "A procedure for patient repositioning and compensation for misalignement between transmission and emission data in PET heart studies," *Journal of Nuclear Medicine*, vol. 34, 1993.

[15] L. Boucher, S. Rodrigue, R. Lecomte, and F. Benard, "Respiratory gating for 3-dimensional PET of the thorax: Feasability and initial results," *Journal of Nuclear Medicine*, vol. 45, no. 2, pp. 214 – 219, 2004.

[16] K. Brown, "Procnostic values of cardic imaging in patients with known or suspected coronary artery disease: comparison of myocardial perfusion imaging, stress echocardiography, and positron emission tomography," *American Journal of Cardiology*, vol. 75, pp. 35D – 41D, 1995.

[17] I. Buvat and I. Castiglioni, "Monte carlo simulations in SPET and PET," *Quartely Journal of Nuclear Medicine*, vol. 46, pp. 48 – 61, 2002.

[18] I. Buvat and D. Lazaro, "Monte carlo simulations in emission tomography and GATE: an overview," *Nuclear Instruments and Methods in Physics research, A*, vol. 569, no. 2, pp. 323 – 329, 2006.

[19] P. Chareonthaitawee, P. Kaufman, O. Rimoldi, and P. Camici, "Heterogeneity of resting and hyperemic myocardial blood flow in healthy humans," *Cardiovascular Research*, vol. 50, pp. 151 – 161, 2001.

[20] J. A. Cooper, P. H. Neumann, and B. K. McCandless, "Effect of patient motion on tomographic myocardial perfusion imaging," *Journal of Nuclear Medicine*, vol. 33, no. 8, pp. 1566 – 1571, 1992.

[21] ——, "Detection of patient motion during tomographic myocardial perfusion imaging," *Journal of Nuclear Medicine*, vol. 34, no. 8, pp. 1341 – 1348, 1993.

[22] K. Could and K. Lipscomb, "Effects of coronary stenosis on coronary flow reserve and resistance," *American Journal of Cardiology*, vol. 34, pp. 48 – 55, 1974.

[23] A. Cuocolo, W. Acampa, M. Imbriaco, N. De Luca, G. I. Iovino, and M. Salvatore, "The many ways to myocardial perfusion imaging," *The quarterly Journal of Nuclear Medicine and Molecular Imaging*, vol. 49, pp. 4 – 18, 2005.

[24] J. Declereck, J. Fldmar, M. Goris, and F. Betting, "Automatic registration and alignment on a template of cardiac stress and rest reoriented SPECT images," *IEEE Transactions on Medical Imaging*, vol. 16, no. 6, pp. 727 – 737, 1997.

[25] P. Descourt, W. Segars, F. Lamare, L. Ferrer, B. Tsui, Y. Bizais, M.Bardiès, and D. Visvikis, "RTNCAT (real time NCAT): Implementing real time physiological movement of voxellized phantoms in GATE," in *In proc. of IEEE Medical Imaging Conference (MIC2006), in press.*, vol. 2, 2000, pp. 87 – 90.

[26] P. Dijkmans, P. Knaapen, G. Sieswerda, E. Aiazian, C. Visser, and A. L. et al, "Quantification of myocardial perfusion using intravenous myocardial contrast echocardiography in healthy volunteers: comparison with positron emission tomography," *Journal of American Society of Echocardiography*, vol. 19, no. 3, pp. 285 – 293, 2006.

[27] R. Eisner, A. Churchwekk, T. Noever, D. Nowak, K. Cloninger, D. Dunn, W. Carlson, J. Oates, J. Jones, D. Morris, H. Liberman, and R. Patterson, "Quantitative analysis of the tomographic thallium-201 myocardial bullseye display: Critical role of correcting for patient motion," *Journal of Nuclear Medicine*, vol. 29, no. 1, pp. 91 – 97, 1988.

[28] A. Frangi, W. Niessen, and M. Viergever, "Three-dimensional modeling for functional analysis of cardiac images: a review," *IEEE Transaction on Medical Imaging*, vol. 20, no. 1, pp. 2 – 25, 2001.

[29] J. Friedman, K. Van Train, J. Maddahi, A. Rozanski, F. Prigent, J. Bietendorf, A. Waxman, and D. Berman, ""Upward creep" of the heart: a frequent source of false-positive reversible defects during thallium-201 stress-redistribution SPECT," *Journal of Nuclear Medicine*, vol. 30, pp. 1718 – 1722, 1989.

[30] S. S. Furuie, G. T. Herman, T. K. Narayan, P. E. Kinahan, J. K. R. M. Lewitt, and S. Matej, "A methodology for testing of statistically significant difference between fully 3D PET reconstruction algorithms," *Physics in Medical Biology*, vol. 39, pp. 341 – 354, 1994.

[31] W. J. Geckle, T. L. Frank, J. M. Links, and L. C. Becker, "Correction for patient and organ movement in SPECT: Application to exercise thallium-201 cardiac imaging," *Journal of Nuclear Medicine*, vol. 29, no. 4, pp. 441 – 450, 1988.

[32] G. Germano, T. Chua, P. B. Kavanagh, H. Kiat, and D. S. Berman, "Detection and correction of patient motion in dynamic and static myocardial SPECT using a multi-detector camera," *Journal of Nuclear Medicine*, vol. 34, no. 8, pp. 1349 – 1355, 1993.

[33] A. C. Guyton and J. E. Hall, *Textbook of Medical Physiology*, 9th ed. W.B. Saunders, 1996.

[34] M. Haddad and G. Porenta, "Impact of reorientation algorithms on quantitative myocardial SPECT perfusion imaging," *Journal of Nuclear Medicine*, vol. 39, no. 11, pp. 1864 – 1869, 1998.

[35] J. Hartiala and J. Knuuti, "Imaging of the heart by MRI and PET," *Annals in Medicine*, vol. 27, pp. 35 – 45, 1995.

[36] E. Hoffman, P. Cutler, W. Digby, and J. Mazziotta, "3D phantom to simulate cerebral blood flow and metabolic images for PET," *IEEE Transaction on Nuclear Science*, vol. 37, pp. 616 – 620, 1990.

[37] C. Hoh, M. Dahlbom, G. Harris, Y. Choi, R. Hawkins, M. Phelps, and J. Maddahi, "Automated iterative three-dimensional registration of positron emission tomography images," *Journal of Nuclear Medicine*, vol. 34, no. 11, pp. 2009 – 2018, 1993.

[38] G. Hutchins, J. Caraher, and R. Raylman, "A region of interest strategy for minimizing resolution distortions in quantitative myocardial PET studies," *Journal of Nuclear Medicine*, vol. 33, no. 6, pp. 1243 – 1250, 1992.

[39] B. Hutton, M. Braun, L. Thurfjell, and D. Lau, "Image registration: an essential tool for nuclear medicine," *European Journal of Nuclear Medicine*, vol. 29, no. 4, pp. 559 – 577, 2002.

[40] A. Hyvärinen, "Fast and robust fixed-point algorithms for independent component analysis," *IEEE Transaction on Neural Networks*, vol. 10, pp. 626 – 634, 1999.

[41] A. Hyvärinen, J. Karhunen, and E. Oja, *Independent Component Analysis*. John Wiley and Sons, 2001.

[42] H. Iida, I. Kanno, S.Miura, M. Murakami, K. Takahashi, Y. ono, F.Shishido, A.Inugami, and N. Tomura, "Measurement of absolute myocardila blood flow

with $H_2^{15}O$ and dynamic positron-emission tomography. strategy for quantification in relation to the partial-volume effect," *Circulation*, vol. 78, pp. 104 – 115, 1988.

[43] H. Iida, I. Kanno, S.Miura, M. Murakami, K. Takahashi, and K. Uemura, "Error analysis of a quantitative cerebral blood flow measurement using $H_2^{15}O$ autoradiography and positron emission tomography, with respect to the dispersion of the input function," *Journal of Cerebral Blood Flow and Metabolism*, vol. 6, pp. 536 – 545, 1986.

[44] H. Iida, C. Rhodes, R. de Silva, L. Araujo, P. Bloomfield, A. Lammertsma, and T. Jones, "Use of left ventricular time activity curve as a noninvasive input function in dynamic oxygen 15 water positron emission tomography," *Journal of Nuclear Medicine*, vol. 32, pp. 1669 – 1677, 1992.

[45] H. Iida, C. Rhodes, R. de Silva, Y. Yamamoto, L. Araujo, A. Maseri, and T. Jones, "Myocardial tissue fraction correction for partial volume effects and measure of tissue viability," *Journal of Nuclear Medicine*, vol. 32, pp. 2169 – 2175, 1991.

[46] P. Jaccard, "Etude comparative de la distribution florale dans une portion des alpes et jura," *Bull. Soc. Vaudeoise Sci. Nat.*, vol. 37, pp. 547 – 579, 1901.

[47] D. Jackson, K. Somers, and H. Harvey, "Similarity coefficients: Measures of co-occurrence and association or simply measures of occurrence?" *The American Naturalist*, vol. 133, no. 3, pp. 436 – 453, 1989.

[48] P. Jannin, E. Krupinski, and S. Warfield, "Guest editorial: Validation in medical image processing," *IEEE Transaction on Medical Imaging*, vol. 25, no. 11, pp. 1405 – 1409, 2006.

[49] P. E. Kinahan, D. W. Townsend, T. Beyer, and D. Sashin, "Attenuation correction for a combined 3D PET/CT scanner," *Medical Physics*, vol. 25, no. 10, 1998.

[50] A. Kivimäki, J. Tohka, M. Anttila, and U. Ruotsalainen, "Extraction of heart volumes from dynamic fdg-pet emission images for movement corrections," *European Journal of Nuclear Medicine and Molecular Imaging*, vol. 31, no. S2, 2004.

[51] G. Klein and R. Huesman, "Four-dimensional processing of deformable cardiac PET data," *Medical Image Analysis*, vol. 6, pp. 29 – 46, 2002.

[52] F. Klocke, M. Baird, T. Bateman, D. Berman, B. Carabello, and M. C. et al., "Acc/aha/asnc guidlines for the clinical use of cardiac radionuclide imaging: executive summary -a report of the america college of cardiology/ american heart association tas on practice guidelines," *Circulation*, vol. 108, pp. 1404 – 1418, 2003.

[53] K. Koshino, N. Kawachi, T. Hayashi, H. Watabe, S. Hasegawa, J. Hatazawa, and H. Iida, "Effects of motion correction on quantification of myocardial blood flow with $^{15}O - H_2O$ PET," in *International Congress Series*, 2004, pp. 106 – 110.

[54] L. Le Meunier, R. Maass-Moreno, J. Carracquillo, W. Dieckmann, and S. Bacharach, "PET/CT imaging: Effect of respiration motion on apparent myocardial uptake," *Journal of Nuclear Cardiology*, vol. 13, no. 6, pp. 821 – 830, 2006.

[55] B. Lee, J. Lee, D. Lee, and S. Choi, "Myocardial blood flow quantification in dynamic PET: an ensamble ICA approach," in *ICANN 2005, Lecture Notes in Computer Science 3697*, 2005, pp. 709 – 714.

[56] J. Lee, J. Ahn, D. Lee, J. Han, M. Jang, J.-K. Chung, M. Lee, and K. Park, "Robust extraction of input function from $H_2^{15}O$ dynamic myocardial postrion emission tomography using independent component analysis," in *In proc. of IEEE Nuclear Science Symposium (NSS99)*, 1999, pp. 990 – 994.

[57] J. Lee, D. Lee, J. Ahn, G. Cheon, S.-K. Kim, J. Yeo, K. Seo, K. Park, J.-K. Chung, and M. Lee, "Blind separation of cardiac components and extraction of input function from $H_2^{15}O$ dynamic myocardial PET usign indepndent component analysis," *Journal of Nuclear Medicine*, vol. 42, no. 6, pp. 938 – 943, 2001.

[58] L. Livieratos, K. Rajappan, L. Stegger, K. Schafers, D. Bailey, and P. Camici, "Respiratory gating of cardiac PET data in list-mode acquisition," *European Journal of Nuclear Medicine and Molecular Imaging*, vol. 33, no. 5, pp. 584 – 588, 2006.

[59] L. Livieratos, L. Stegger, P. Bloomfield, K. Schafers, D. Bailey, and P. Camici, "Rigid-body transformation of list-mode projection data for respiratory motion correction in cardiac pet," *Physics in Medicine and Biology*, vol. 50, no. 14, pp. 3313 – 3322, 2005.

[60] C. Loghin, S. Sdringola, and K. Gould, "Common artefacts in PET myocardial perfusion images due to attenuation-emission misregistration: clinical significance, causes and solutions," *Journal of Nuclear Medicine*, vol. 45, pp. 1029 – 1039, 2004.

[61] C. Lorenz, J. Pastorek, and J. Bundy, "Delineation of normal human left ventricular twist throughout systole by tagged cine magnetic resonance imaging," *Journal of Cardiovascular Magnetic Resonance*, vol. 2, no. 2, pp. 97 – 108, 2000.

[62] F. Maes, A. Collignon, D. Vandermeulen, G. Marchal, and P. Suetens, "Multimodality image registration by maximization of mutual information," *IEEE Transaction on Medical Imaging*, vol. 16, no. 2, pp. 187 – 198, 1997.

[63] M. Magadán-Méndez, A. Kivimäki, and U. Ruotsalainen, "ICA separation of functional components from dynamic cardiac PET data," in *In Proc. of IEEE Medical Imaging conference (MIC2003)*, 2003, pp. 2618 – 2622.

[64] ——, "Testing of the sensitivity of ICA separation to noise with simulated cardiac PET data," in *Proc. of Finnish Signal Processing Symposium*, Tampere, Finland, 2003, pp. 17 – 21.

[65] J. Maintz and M. Viergever, "An overview of medical image registration methods," *Medical Image Analysis*, vol. 2, no. 1, pp. 1 – 36, 1998.

[66] T. Mäkelä, "Data registration and fusion for cardiac applications," Ph.D. dissertation, Helsinki University of Technology, 2003.

[67] T. Mäkelä, P. Clarysse, O. Sipilä, N. Pauna, Q. Pham, T. Katila, and I. Magnin, "A review of cardiac image registration methods," *IEEE Transactions on Medical Imaging*, vol. 21, no. 9, pp. 1011 – 1021, 2002.

[68] A. Martinez-Möller, M. Souvatzoglou, N. Navab, M. Schwaiger, and S. Nekolla, "Artifacts from misaligned CT in cardiac perfusion PET/CT studies: Frequency, effects, and potential solutions," *Journal of Nuclear Medicine*, vol. 48, no. 2, pp. 2188 – 2193, 2007.

[69] M. McCord, S. Bacharach, R. Bonow, V. Dilsizian, A. Cuocolo, and N. Freedman, "Misalignment between PET transmission and emission scans: its effect on myocardial imaging," *Journal of Nuclear Medicine*, vol. 33, no. 6, pp. 1209 – 1214, 1992.

[70] A. Naum, M. S. Laaksonen, H. Tuunanen, V. Oikonen, M. Teräs, J. Kemppainen, M. J. Järvisalo, P. Nuutila, and J. Knuuti, "Motion detection and correction for dynamic o^{15}-water myocardial perfusion pet studies," *European Journal of Nuclear Medicine and Molecular Imaging*, vol. 32, no. 12, pp. 1378 – 1383, 2005.

[71] S. Nehmeh, Y. Erdi, T. Pan, E. Yorke, G. Mageras, K. Rosenzweig, H. Schoode, H. Mostafavi, O. Squire, A. Pevsner, S. Larson, and J. Humm, "Quantification of respiratory motion during 4D-PET/CT acquisition," *Medical Physics*, vol. 31, no. 6, pp. 1333 – 1338, 2004.

[72] V. Oikonen, "Model equations for myocardial perfusion studies with $[^{15}O]H_2O$ PET," Turku PET Centre, Tech. Rep., 2002.

[73] K. Okrainec, D. Banerjee, and M. J. Eisenberg, "Coronary artery disease in the developing world," *American Heart Journal*, vol. 148, pp. 7 – 15, 2003.

[74] S. Pallotta, M. Gilardi, V. Bettinardi, G. Rizzo, C. Landoni, G. Striano, R. Madi, and F. Fazio, "Application of a surface matching image registration technique

to the correlation of cardiac studies in positron emission tomography by transmission images," *Physics in Medicine and Biology*, vol. 40, pp. 1695 – 1708, 1995.

[75] J. Park, D. Metaxas, A. Young, and L. Axel, "Deformable models with parameter functions for cardiac motion analysis form tagged MRI data," *IEEE Transaction on Medical Imaging*, vol. 15, pp. 278 – 289, 1996.

[76] D. Pennell and E. Prvulovich, *Clinician's guide to nuclear medicine: nuclear cardiology*. Hatfield: Impact Healthcare, 1995.

[77] J. Pluim, J. Maintz, and M. Viergever, "Mutual-information-based registration of medical images: a survey," *IEEE Transacation on Medical Imaging*, vol. 22, pp. 986 – 1004, 2003.

[78] P. Pretarious, W. Xia, M. King, B. Tsui, and K. Lacroix, "A mathematical model of motion of the heart for use in generating source and attenution maps for simulating emission imaging," *Medical Physics*, vol. 26, pp. 2323 – 2332, 1999.

[79] P. Pretarious, W. Xia, M. King, B. Tsui, T.-S. Pan, and B. Villegas, "Evaluation of the righ and left ventricular volume and ejection fraction using a mathematical cardiac torso phantom," *Journal of Nuclear Medicine*, vol. 38, no. 10, 1997.

[80] J. Räsänen, "Testing of independent component analysis on the separation of tissues on dynamic cardiac pet images," Master's thesis, Tampere University of Technology, Institute of Signal Processing, Tampere, Finland, 2006.

[81] A. Reilhac, G. Batan, C. Michel, C. Grova, J. Tohka, D. Collins, N. Costes, and A. Evans, "PET-SORTEO: validation and development of database of simulated pet volumes," *IEEE Transactions on Nuclear Science*, vol. 52, no. 5, pp. 1321 – 1328, 2005.

[82] A. Reilhac, C. Lartizien, N. Costes, S. Sans, C. Comtat, R. Gunn, and A. Evans, "PET-SORTEO: A Monte Carlo-based simulator with high count rate capabilities," *IEEE Transactions on Nuclear Science*, vol. 51, no. 1, pp. 46 – 52, 2004.

[83] B. Reutter, S. Lim, R. Huesman, P. Coxson, G. Klein, and T. Budinger, "Cardiac creep during rest/stress myocardial perfusion studies - patient motion and lung air distribution," *Journal of Nuclear Medicine*, vol. 37, no. 5 suppl, p. 131P, 1996.

[84] H. Schelbert, "The usefulness of positron emission tomography," *Current Problems in Cardiology*, vol. 23, no. 2, pp. 71 – ´120, 1998.

[85] J. Schwitter, T. DeMarco, S. Kneifel, G. von Schulthess, M. Jörg, and H. Arheden, "A magnetic resonance based assessment of global coronary flow and flow

reserve and its relation to left ventricular functional parameters: Comparison with positron emission tomography," *Circulation*, vol. 101, pp. 2696 – 2702, 2000.

[86] U. Sechtem, B. Sommerhoff, W. Markiewicz, R. White, M. Cheitlin, and C. Higgins, "Regional left ventricular wall thickening by magnetic resonance imaging: evalution in normal persons and patients with global and regional dysfunction," *The America Journal of Cardiology*, vol. 59, pp. 145 – 151, 1987.

[87] W. Segars, "Development and application of the new dynamic NURBS-based cardiac-torso NCAT phantom," Ph.D. dissertation, University of North Carolina, Chapel Hill, NC, 2001.

[88] W. Segars, D. Lalush, and B. Tsui, "Modelling respiratory mechanics in the MCAT phantoms," *IEEE Transaction on Nuclear Science*, vol. 48, pp. 89 – 97, 2001.

[89] T. Sharir, D. Berman, P. Waechter, P. K. J. Areeda, J. Gerlach, X. Kang, and G. Germano, "Quantitative analysis of regional motion and thickening be gated myocardial perfusion SPECT: Normal heterogenoity and criteria for abnormality," *Journal of Nuclear Medicine*, vol. 42, no. 11, 2001.

[90] G. Shechter, J. Resar, and E. McVeigh, "Displacement and velocity of the coronary arteries: cardiac and respiratory motion," *IEEE Transaction on Medical Imaging*, vol. 25, no. 3, pp. 369 – 375, 2006.

[91] P. Slomka, G. Hurwitz, J. Sephenson, and T. Cradduck, "Automated alignment and sizing of myocardial stress and rest scans to three-dimensional normal templates using an image registration algorithm," *Journal of Nuclear Medicine*, vol. 36, no. 6, pp. 1115 – 1122, 1994.

[92] P. Slomka, H. Nishina, D. Berman, X. Kang, J. Friedman, S. hayes, U. Aladl, and G. Germano, "Automatic quantification of myocardial perfusion stress-rest change: a new measure of ischemia," *Journal of Nuclear Medicine*, vol. 45, no. 2, pp. 183 – 191, 2004.

[93] M. Smith, "The effect of contraction and twis on myocardial PET and SPECT image resolution: a methematical phantom study," *IEEE transactions on nuclear science*, vol. 47, pp. 1646 – 1654, 2000.

[94] C. Studholm, D. Hill, and D. Hawkes, "An overlap invariant entropy measure of 3D medical image alignment," *Pattern Recognition*, vol. 32, pp. 71 – 86, 1999.

[95] M. M. Ter-Pogossian, S. R. Bergmann, and B. E. Sobel, "Influence of cardiac and respiratory motion on tomographic reconstructions of the heart: implications for quantitative nuclear cardiology," *Journal of Computer Assisted Tomography*, vol. 6, no. 6, pp. 1148 – 1155, 1982.

[96] J. Tohka, A. Kivimäki, A. Reilhac, J. Mykkänen, and U. Ruotsalainen, "Assessment of brain surface extraction from PET images using Monte Carlo simulations," *IEEE Transaction on Nuclear Science*, vol. 51, no. 5, pp. 2641 – 2648, October 2004.

[97] J. Tohka and J. Mykkänen, "Deformable mesh for automated surface extraction from noisy images," *International Journal of Image Graphics*, vol. 4, no. 3, pp. 405– 432, 2004.

[98] T. Turkington, T. DeGrado, M. Hanson, and R. Coleman, "Alignment of dynamic cardiac pet images for correction of motion," *IEEE Transactions on Nuclear Science*, vol. 44, pp. 235 – 242, 1997.

[99] J. van den Hoff, W. Burchert, W. Muller-Schauenbrug, G.-J. Meyer, and H. Hundeshagen, "Accurate local blood flow measurements with dynamic PET: fast determination of input function delay and dispersion by multilinear minimization," *Journal of Nuclear Medicine*, vol. 34, no. 10, pp. 1770 – 1777, 1993.

[100] A. Veress, W. Segars, J. Weiss, B. Tsui, and G. Gullberg, "Normal and pathological NCAT image and phantom data based on physiologically realistic left ventricle finite-element models," *IEEE Transaction on Medical Imaging*, vol. 25, no. 12, 2006.

[101] V. Walimbe, V. Zagrodsky, S. Raja, W. Jaber, F. DiFilippo, M. Carcia, R. Brunken, J. Thomas, and R. Shekhar, "Mutual information-based multimodality registration of cardiac ultrasound and SPECT images: a preliminary investigation," *The International Journal of Cardiovascular Imaging*, vol. 19, pp. 483 – 494, 2003.

[102] Y. Wang, S. Riederer, and R. Ehman, "Respiratory motion of the heart: kinematics and the implications for spatial resolution in coronary imaging," *Magnetic Resonance in Medicine*, vol. 33, pp. 713 – 719, 1995.

[103] H. Watabe, H. Jino, N. Kawachi, N. Teramoto, T. Hayasi, Y. Ohta, and H. Iida, "Development of motion correction technique for PET study using optical tracking system," in *Quantification in Biomedical Imaging with PET and MRI: Proceedings of the International Workshop on Quantification in Biomedical Imaging with PET and MRI, International Congress Series, volume 1265*, January 2004, pp. 31–38.

[104] ——, "Parametric imaging of myocardium blood flow with O^{15}-water and PET using the basis function method," *Journal of Nuclear Medicine*, vol. 46, pp. 1219 – 1224, 2005.

[105] W. Wells III, W. Grimson, R. Kikinis, and F. A. Jolesz, "Adaptive segmentation of MRI data," *IEEE Transactions on Medical Imaging*, vol. 15, no. 4, pp. 429 – 442, 1996.

[106] J. Wong, C. Studholme, D. Hawkes, and M. Maisey, "Evaluation of the limits of visual detection of image misregistration in a brain fluorine-18 fluorodeoxyglucose PET-MRI study," *European Journal of Nuclear Medicine*, vol. 24, no. 6, pp. 642 – 650, 1997.

[107] R. Woods, "Validation of registration accuracy," in *Handbook of medical imaging: processing and analysis*, I. Bankman, Ed. Academic Press, USA, 1999, pp. 491 – 497.

[108] E. Xu, N. Mullani, K. Gloud, and W. Anderson, "A segmented attenuation correction for PET," *Journal of Nuclear Medicine*, vol. 32, 1991.

[109] J. Yu, F. Fahey, B. Harkness, H. Cage, C. Eades, and J. Keyes, "Evaluation of emission-transmission registration in thoracic PET," *Journal of Nuclear Medicine*, vol. 35, no. 11, pp. 1777 – 1781, 1994.

[110] H. Zaidi, M. Diaz-Gomex, A. Boudraa, and D. Slosman, "Fuzzy clustering-based attenuation correction in whole-body PET imaging," *Physics in Medicine and Biology*, no. 47, pp. 1143 – 1160, 2002.

[111] H. Zaidi, A. Scheurer, and C. Morel, "An object oriented Monte Carlo simulator for 3D cylinderical positron tomographs," *Computer Methods and Programs in Biomedicine*, no. 58, pp. 133 – 145, 1999.

[112] E. Zerhouni, D. Parish, W. Rogers, and A. Yang, "Human heart: tagging with MR imaging - a method for nonivasive assessment of myocardial motion," *Radiology*, vol. 169, pp. 59 – 63, 1988.

[113] I. Zubal, C. Harrell, E. Smith, Z. Rattner, G. Gindi, and P. Hoffer, "Computerized three-dimensional segmented human anatomy," *Medical Physics*, vol. 21, no. 2, pp. 299 – 302, 1994.

Publications

Publication I

A. Juslin, A. Reilhac, M. Magadan-Mendez, E. Alban, J. Tohka and U. Ruotsalainen, "Assessment of separation of functional components with ICA from dynamic cardiac perfusion PET phantom images for volume extraction with deformable models," in *Third International Conference on Functional Imaging and Modeling of the Heart (FIMH'05)*, Lecture Notes in Computer Science (LNCS), 3504, 2005, pp. 338–347.

Publication II

A. Juslin, and J. Tohka, "Unsupervised segmentation of cardiac PET transmission images for automatic heart volume extraction," in *Proceedings of the 28th Annual International Conference of the IEEE Engineering in Medicine and Biology Society (EMBC'06)*, New York, USA, August 30 – September 3, 2006, pp. 1077–1080.

Publication III

M. Magadan-Mendez, A. Juslin, SV. Nesterov, J. Knuuti, and U. Ruotsalainen, "ICA based automatic segmentation of dynamic $H_2^{15}O$ cardiac PET images," in *IEEE Transaction on Information Technology in Biomedicine*, accepted, 2007.

Publication IV

A. Juslin, J. Lötjönen, SV. Nesterov, J. Knuuti, and U. Ruotsalainen,"Alignment of 3-dimensional cardiac structures in O-15-labeled water PET emission images with mutual information," *Journal of Nuclear Cardiology*, vol 14, no.1, 2007, pp. 82–91, .

Publication V

A. Juslin, J. Tohka, J. Lötjönen, and U. Ruotsalainen, "Comparison of image segmentation and registration based methods for analysis of misaligned dynamic $H_2^{15}O$ cardiac PET images ," in *Proceedings of the IEEE Medical Imaging Conference (MIC2006)*, San Diego, USA, December 1–4, 2006, pp. 3200–3204.